

SOURCE  
DATATRANSPARENT  
PROCESS

# F-domain valency determines outcome of signaling through the angiopoietin pathway

Yan Ting Zhao<sup>1,2,3,†</sup> , Jorge A Fallas<sup>1,4,†</sup> , Shally Saini<sup>1,2</sup> , George Ueda<sup>1,4</sup> ,  
Logeshwaran Somasundaram<sup>1,2</sup> , Ziben Zhou<sup>1,2</sup> , Infencia Xavier Raj<sup>1,2</sup> , Chunfu Xu<sup>1</sup> ,  
Lauren Carter<sup>1,4</sup> , Samuel Wrenn<sup>1,4</sup>, Julie Mathieu<sup>2,5</sup> , Drew L Sellers<sup>2,6,\*</sup> , David Baker<sup>1,4,6,\*\*</sup> &  
Hannele Ruohola-Baker<sup>1,2,3,6,\*\*\*</sup>

## Abstract

Angiopoietins 1 and 2 (Ang1 and Ang2) regulate angiogenesis through their similar F-domains by activating Tie2 receptors on endothelial cells. Despite the similarity in the underlying receptor-binding interaction, the two angiopoietins have opposite effects: Ang1 induces phosphorylation of AKT, strengthens cell–cell junctions, and enhances endothelial cell survival while Ang2 can antagonize these effects, depending on cellular context. To investigate the molecular basis for the opposing effects, we examined the phenotypes of a series of computationally designed protein scaffolds presenting the Ang1 F-domain in a wide range of valencies and geometries. We find two broad phenotypic classes distinguished by the number of presented F-domains: Scaffolds presenting 3 or 4 F-domains have Ang2-like activity, upregulating pFAK and pERK but not pAKT, while scaffolds presenting 6, 8, 12, 30, or 60 F-domains have Ang1-like activity, upregulating pAKT and inducing migration and vascular stability. The scaffolds with 6 or more F-domains display super-agonist activity, producing stronger phenotypes at lower concentrations than Ang1. Tie2 super-agonist nanoparticles reduced blood extravasation and improved blood–brain barrier integrity four days after a controlled cortical impact injury.

**Keywords** Akt; angiogenesis; angiopoietins; self-assembled oligomer protein; Tie2

**Subject Categories** Biotechnology & Synthetic Biology; Signal Transduction; Vascular Biology & Angiogenesis

**DOI** 10.15252/embr.202153471 | Received 18 June 2021 | Revised 9 September 2021 | Accepted 16 September 2021 | Published online 26 October 2021

**EMBO Reports (2021) 22: e53471**

## Introduction

Ang1 and Ang2 both contain a Tie2-binding carboxy-terminal fibrinogen-like domain (F), a coiled-coil domain, and an amino-terminal super clustering domain for multimerization (Davis *et al*, 2003). The binding modes of the Ang1 and Ang2 F-domains to Tie2 are very similar (carbon alpha r.m.s.d. of 0.8 Å; pdb id 4k0v (Yu *et al*, 2013) and 2gy7 (Barton *et al*, 2006)), and they have nearly identical tertiary structure (Yu *et al*, 2013) and similar Tie2-binding affinity (Maisonpierre *et al*, 1997), and thus, it has been speculated that differences in Ang/Tie2 signaling outputs produced by Ang1 and Ang2 are due to differences in their oligomerization state. Crystal structures of the Tie2 extracellular region (ECR) coupled with solution X-ray scattering experiments have shown that the ECR forms a dimer in solution and suggest two different receptor association modes involving the membrane-proximal FNIII domains (Souma *et al*, 2016; Leppänen *et al*, 2017; Moore *et al*, 2017), and it has been proposed that binding of multivalent Ang1-like ligands leads to the generation of a regular lattice of Tie2 receptors from constitutively formed dimers (Leppänen *et al*, 2017; Moore *et al*, 2017). EM characterization of the Ang1 and Ang2 oligomerization states suggests greater tendency of the former to self-associate (Davis *et al*, 2003; Cho *et al*, 2004; Kim *et al*, 2005), which has been proposed to stem from a cysteine residue in Ang1 that is not present in Ang2 (Kim *et al*, 2005). Constructs displaying multiple F-domains, such as Comp-Ang (Cho *et al*, 2004), have been generated that have Ang1-like activity, but correlating receptor-binding valency to signaling output is not straightforward since both Ang1 or Ang2 (Kim *et al*, 2005), an Ang1 surrogate (Davis *et al*, 2003), and Comp-Ang (Cho *et al*, 2004) can occupy a range of oligomeric states. Similarly, an anti-Ang antibody, ABTAA, potentiates Tie2 activation, but the oligomerization state of the active signaling complexes is unclear

1 Department of Biochemistry, University of Washington, Seattle, WA, USA  
 2 Institute for Stem Cell and Regenerative Medicine, University of Washington, Seattle, WA, USA  
 3 Oral Health Sciences, School of Dentistry, University of Washington, Seattle, WA, USA  
 4 Institute for Protein Design, University of Washington, Seattle, WA, USA  
 5 Department of Comparative Medicine, University of Washington, Seattle, WA, USA  
 6 Department of Bioengineering, University of Washington, Seattle, WA, USA  
 \*Corresponding author. Tel: +1 206 616 8023; E-mail: drewfus@uw.edu  
 \*\*Corresponding author. Tel: +1 206 616 7542; E-mail: dabaker@uw.edu  
 \*\*\*Corresponding author. Tel: +1 206 543 8468; E-mail: Hannele@uw.edu  
 †These authors contributed equally to this work

(Han *et al*, 2016). Further complicating the picture, work with chimeric mouse angiopoietins generated by swapping the F-domains of Ang1 and Ang2 suggested the F-domain is the determinant for Tie2 activation, not the oligomeric state (Procopio *et al*, 1999).

Here we generate and characterize computationally designed protein scaffolds presenting the Ang1 F-domain in a wide range of valencies and geometries and show that scaffolds presenting 3 or 4 F-domains have Ang2-like activity, while scaffolds presenting 6, 8, 12, 30, or 60 F-domains have Ang1-like activity. The Tie2 agonist nanoparticles improved blood–brain barrier integrity four days after a controlled cortical impact injury.

## Results

We set out to systematically investigate the molecular basis of the Ang1 and Ang2 signaling differences by generating a series of computationally designed ligands which display F-domains in a wide range of valencies (3, 4, 6, 8, 12, 30, and 60 copies of F-domain) and symmetries (cyclic, tetrahedral, and icosahedral) (Fig 1A). We employed previously designed trimeric (H3, Tet1-A, Tet1-A.2, and Icos1-A), tetrameric (C4 and AkC4), hexameric (H6), octameric (H8) cyclic oligomers with 3, 4, 6, and 8 subunits, and tetrahedral (Tet1 and Tet2) and icosahedral (Icos1 and Icos2) with 12 and 60 copies of F-domains, respectively (Bale *et al*, 2016; Fallas *et al*, 2017; Xu *et al*, 2020). To ensure that the F-domain was identical across all the different presentation formats, we covalently conjugated SpyTagged F-domain to a SpyCatcher domain fused to the N- or C-terminus of the designed scaffold subunits (Fig 1A and Appendix Fig S1A) (Zakeri *et al*, 2012). To examine the effect of F-domain spacing independent of oligomerization state, we produced four different trimeric configurations in which the distance between the F-domain attachment points ranged from 2.2 nm to 8.0 nm. Protein sequences and details on protein production, purification, conjugation, and characterization are described in the methods and supporting information sections (Appendix Fig S4A–D and Appendix Table S1). The SpyTag–SpyCatcher conjugation efficiency was ~80% for the tetrameric scaffolds and 90% or greater for all the remaining scaffolds (Fig 1B). The homogeneity of the designed scaffolds is illustrated for F-domain-conjugated Icos1 in Fig 1C—the negative stain electron micrographs show spherical particles of the expected size (~30nm) and shape with small spikes corresponding to the SpyCatcher domain displayed on the particle surface.

## Akt phosphorylation correlates with F-domain valency

We evaluated the activity of F-domain scaffolds by determining their signaling profiles in Human Umbilical Vein Endothelial Cells (HUVECs). To set a baseline for these studies, serum-starved HUVECs were treated with Ang1 or Ang2 (18nM) for 15 min, and the activation of downstream signaling pathways was analyzed by western blot. Consistent with previous studies, Ang1 treatment increased phosphorylation of AKT (S473), FAK (Y397), and ERK1/2 (T202, Y204), whereas Ang2 only activated FAK and ERK (Fig 1D).

The multivalent F-domain displaying designed scaffolds were incubated with HUVEC cells, and protein lysates were analyzed for AKT (S473), ERK1/2 (T202/Y204), FAK (Y397), and Tie2 (Y992) phosphorylations using immunoblotting. We observed a significant increase in Tie2 phosphorylation following F-domain scaffold administration, suggesting that the synthetic ligands act through similar pathways as natural ligands (Appendix Fig S5A and B). The differences in AKT activation between the different valencies were notable. The four trimeric scaffolds failed to activate AKT, as did the tetrameric scaffolds (Fig 2A, D, E, H, I, L, and Appendix Fig S1C and D). In contrast, all the scaffolds displaying six or more SpyCatcher domains strongly activated AKT. To confirm that the F-domain scaffolds signal through Tie2 receptors, we knocked down Tie2 expression in HUVECs using siRNA. This significantly reduced H8-dependent pAKT levels compared with cells stimulated with H8 but without siRNA transfection (Fig 2Q and R), showing that the multivalent F-domain scaffolds act through the Tie2 receptor. The distance between F-domains in the scaffolds had relatively little impact on signaling—the range of distances among the trimeric and tetrameric scaffolds was similar to those of the higher valency scaffolds. Several direct comparisons highlight the importance of F-domain valency over that of geometry. First, the series of scaffolds H3, H6, and H8 have nearly identical geometry (cyclic helical bundles), but the trimeric H3 failed to induce AKT phosphorylation while the hexameric H6 and octameric H8 both strongly induced phosphorylation (Fig 2A and D). The nanoparticles are comprised of two self-assembling components, one of which is conjugated to the F-domain using SpyTag and SpyCatcher as described previously. The F-domain-conjugated nanoparticle components Tet1-A and Icos1-A failed to activate AKT on their own (Fig 2E and I). However, when combined with the partner nanoparticle component which results in a tetrahedral (Tet1 and Tet2) or icosahedral (Icos1 and Icos2) assembly, respectively, both nanoparticles strongly activate AKT. While there was a strong effect of valency on

**Figure 1. Computationally designed scaffolds present Ang1 F-domain in wide range of geometries and valencies.**

- A Designed F-domain scaffold structures. Red and purple dots indicate N- and C-terminal sites of F-domain conjugation, respectively. N is the maximum number of conjugated F-domains, and the dashed lines are the distance between F-domain conjugation sites. Top two rows: Cyclic homo-oligomers. The trimeric nanocage subunits Icos1-A, Tet1-A, and Tet1-A.2 allow precise testing of the effect of valency on signaling independent of geometry as they can be tested as trimers alone or as nanocages upon addition of the other component of these two-component nanoparticles. C4 and AkC4 are tetrameric scaffolds, and H3, H6, and H8 are helical bundle scaffolds with nearly identical geometry but different valency. Third row: Tetrahedral nanoparticle scaffolds Tet1 and Tet2. Fourth row: Icosahedral nanoparticles. Icos1 and Icos2 present sixty copies of the F-domain on the trimer and pentamer subunits, respectively.
- B Average conjugation efficiency maximum number of F-domains for each scaffold.
- C Negative stain electron micrograph of Icos1 scaffold with 60 F-domain conjugation sites. Scale bar is 1,000 nm.
- D Serum-starved HUVECs were stimulated with 18 nM of angiopoietins or PBS (vehicle) for 15 min, and phosphorylation levels were analyzed by immunoblotting for pAKT(S473), pERK1/2 (T202/Y204), pFAK(Y397), and  $\beta$ -Actin.

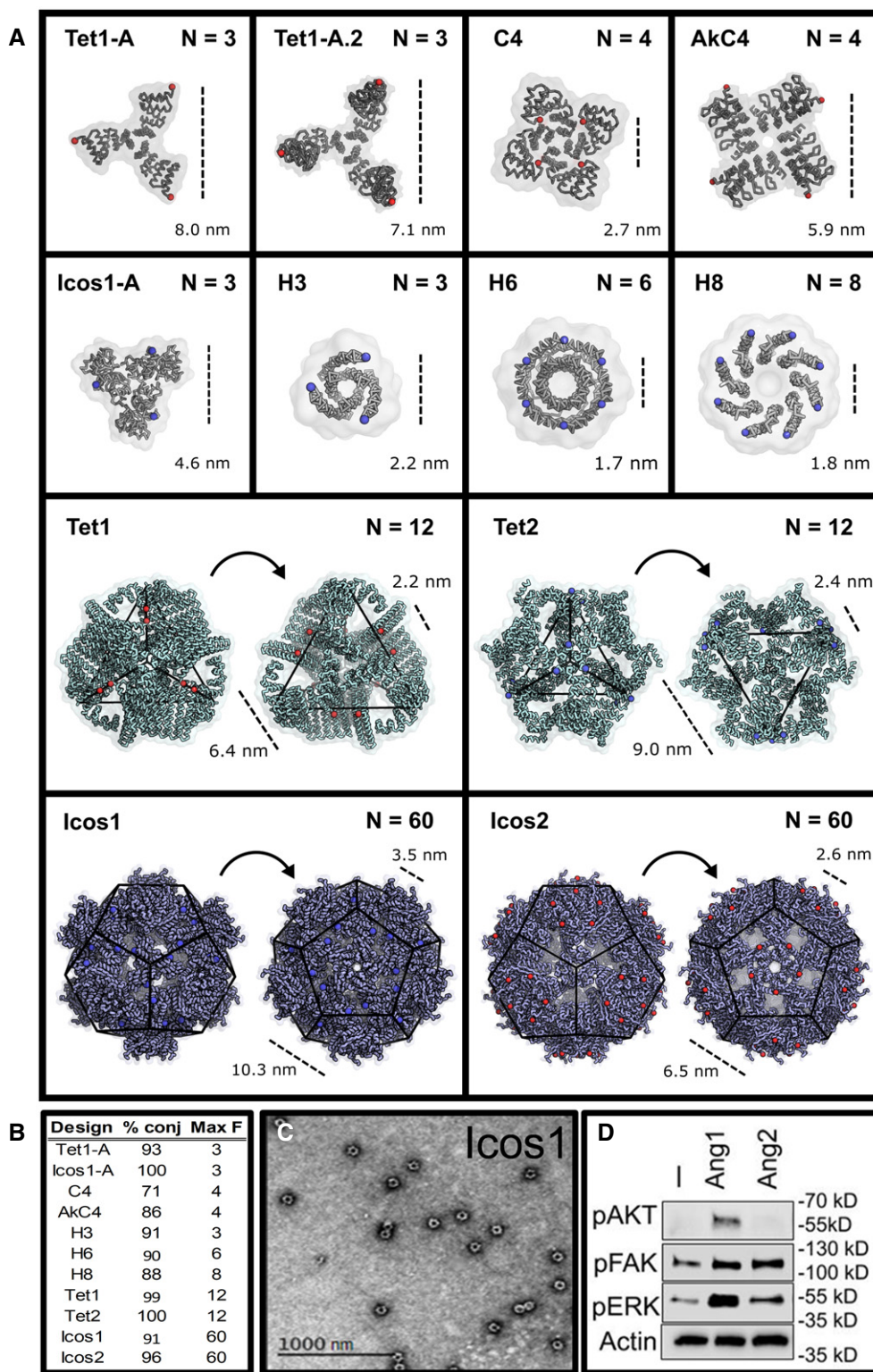


Figure 1.

AKT activation, almost all scaffolds upregulated FAK (Fig 2C, G and K) and ERK phosphorylation (Fig 2B, F and J). FAK phosphorylation appears to be somewhat sensitive to geometry as Tet1-A activated FAK phosphorylation more than the other trimeric and tetrameric

constructs (Fig 2G). These results suggest that induction of clusters of 3–4 F-domains is sufficient to induce phosphorylation of FAK and ERK, but phosphorylation of AKT requires clustering of six or more F-domains.

To compare the potency of the synthetic ligands to Ang1 and assess the effect of multivalency on cell binding affinity/avidity, we investigated the concentration dependence of AKT activation for a subset of scaffolds alongside Ang1 and Ang2. Serum starved HUVECs were treated with H3, H6, H8, Icos1, or Icos2, and AKT activation was analyzed using immunoblotting (Fig 2M and N and

Appendix Fig S1F–L). All scaffolds with six or more copies of F-domain had lower half-maximal ( $EC_{50}$ ) AKT activation than Ang1; the H8 scaffold exhibited the lowest  $EC_{50}$  (1.4 nM F-domain), 19-fold lower than Ang1 ( $EC_{50} = 27$  nM F-domain). AKT activation was much less variable with the synthetic scaffolds than Ang1. The higher valency designed scaffolds, on average, produced a higher

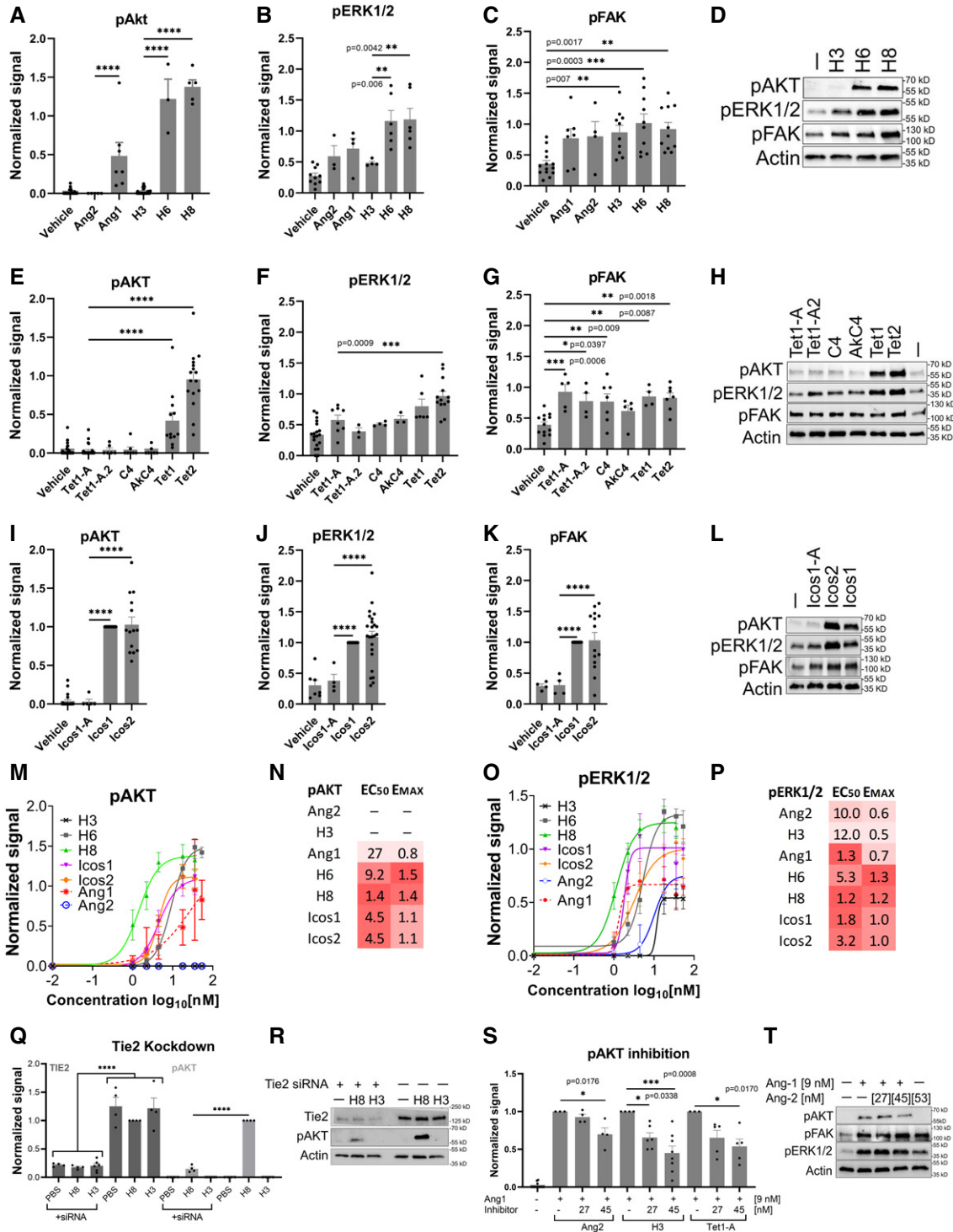


Figure 2.

**Figure 2. F-domain valency determines level of activation of AKT phosphorylation.**

- A–L Serum-starved HUVECs were stimulated with designed scaffolds normalized to 18 nM of F-domains for 15 min and analyzed by immunoblotting for pAKT (S473), pERK1/2 (T202/Y204), and pFAK (Y397) phosphorylations. (A, E, I) pAKT, (B, F, J) pERK1/2, and (C, G, K) pFAK phosphorylation levels were quantified and normalized to Icos-cage signaling levels. Appendix Fig S1B shows the detection of two bands expected for pERK1/2. Representative immunoblot gels of cells stimulated with or without scaffolds at 18 nM of F-domain: (D) helical bundles, (H) trimeric and tetrameric homo-oligomers and tetrahedral nanocages, (L) Icosahedral nanocages and trimeric subunit.
- M–P Dose–response curves,  $EC_{50}$ , and  $E_{MAX}$  for pAKT and pERK1/2 activation. The curves,  $EC_{50}$  and  $E_{MAX}$  values are calculated using Prism, GraphPad. (N, P) Darker red color indicates lower  $EC_{50}$  and higher  $E_{MAX}$  values.
- Q, R Quantification (Q) and representative gel (R) for Tie2 knockdown using 40 nM of siRNA before starvation and F-domain scaffold at 18 nM of F-domain or PBS stimulation.
- S, T Quantification (S) and representative gel (T) for inhibition of Ang1-dependent pAKT signaling by Ang2, H3, Tet1-A, or Icos1-A; pAKT band intensities were normalized to Ang1-dependent pAKT level). Representative immunoblots for H3, Tet1-A, and Icos1-A competition experiments are in Appendix Fig S1M–O. Quantification of pERK1/2 and pFAK level for the competition assay is in Appendix Fig S1P and Q. Partial valency analysis of icosahedral nanocages is in Appendix Fig S1R–T.

Data information: Each point on all graphs represents a biological replicate,  $n > 3$ , bars represent the mean  $\pm$  SEM. One-way ANOVA with Bonferroni test was used for multiple comparisons to calculate  $P$ -values. (\*\*\*) indicates  $P < 0.0001$ .  $P$ -values are also indicated in Appendix Table S2.

level of maximum pAKT (Avg.  $E_{MAX} = 1.3$ ) compared with Ang1 ( $E_{MAX} = 0.8$ ). No AKT phosphorylation was observed in H3 titrations, even at high concentrations.

We similarly compared dose–response curves for activation of ERK1/2 phosphorylation by the designed scaffolds with those of Ang1 and Ang2 (Fig 2O and P). The designed high valency F-domain scaffolds activated pERK1/2 to a greater extent (higher  $E_{MAX}$ ) than Ang1 and Ang2. H8 was again the most active ( $E_{MAX} = 1.2$ ) compared with Ang1 ( $E_{MAX} = 0.7$ ) and Ang2 ( $E_{MAX} = 0.6$ ). The H8 scaffold also had the lowest  $EC_{50}$  (1.2 nM F-domain). The efficiency and maximum signaling level of H3 and Ang2 to activate pERK1/2 are very similar with  $E_{MAX} = 0.5$  and 0.6, respectively, and  $EC_{50} = 12$  and 10 nM F-domain, respectively.

Overall, the designed, high valency F-domain scaffolds behave as super-agonists that activate the Tie2 pathway more strongly than Ang1 (for pAKT and pERK activations) or Ang2 (for pERK activation); the synthetic ligands are also considerably more robust.

**Trimeric scaffolds are Tie2-dependent pAKT antagonists**

Ang2 antagonizes Ang1 activity (Maisonpierre *et al*, 1997; Yuan *et al*, 2009), and to explore the mechanism of this antagonism, we investigated the effect of the F-domain scaffolds that do not activate pAKT on Ang1-induced pAKT phosphorylation. Consistent with expectation, in the HUVEC system, there was considerable attenuation of Ang1-dependent pAKT signaling in the presence of higher concentrations of Ang2 (9 nM Ang1 and 45 nM Ang2; Fig 2S and T). We found that the trimeric scaffolds H3 and Tet1-A reduced Ang1-induced pAKT expression at 27 and 45 nM F-domain concentrations (Appendix Fig S1M–O). H3 was more effective than Ang2 in reducing Ang1 signaling at 45 nM F-domain. We conclude that the trimeric scaffolds cannot activate pAKT but can block Ang1-dependent pAKT activation. The simplest explanation for this observation is that the F-domain scaffolds bind to available Tie2 receptors, blocking Ang1-induced activation by direct competition for receptor-binding sites, but we cannot rule out the possibility that this is cell type dependent.

**Scaffolds with six or more F-domains increase endothelial cell migration *in vitro***

Angiogenesis requires sprouting, proliferation, and migration of endothelial cells (Mazurek *et al*, 2017), and activation of Tie2 by

Ang1 promotes cell migration (Fukuhara *et al*, 2008; Saharinen *et al*, 2008; Xue & Hemmings, 2013). To evaluate the capacity of the F-domain scaffolds to promote wound healing, we evaluated them using a commonly used *in vitro* cell migration assay (Liang *et al*, 2007). Confluent HUVECs were scratched in the center of the dish to mimic a wound and treated with scaffolds at 18 nM of F-domain for 12 h (Fig 3A). The change in the model wound area was followed to assess the extent of cell migration (Fig 3B). H6, H8, Icos1, and Icos2 increased cell migration (2- to 3-fold) compared with the vehicle ( $P < 0.0001$ ). H8 and Icos1 increased considerably more migration than Ang1 ( $P < 0.05$ ). In contrast, H3, Tet1-A, C4, and Icos1-A, like Ang2 (Harfouche & Hussain, 2006), did not increase cell migration (Fig 3C and Appendix Fig S2A).

**High valency F-domain scaffolds stabilize HUVEC cell tubules**

We investigated the effect of the F-domain scaffolds on HUVEC tube formation, a simple but well-established *in vitro* angiogenesis assay (DeCicco-Skinner *et al*, 2014). HUVECs were plated on 100% Matrigel and incubated with F-domain scaffolds at 90 nM of F-domain for 24 h; thereafter, the scaffolds were removed, and the vascular stability was measured at 48- or 72-h timepoints (Fig 3D). Tubule networks were imaged, and the number of nodes, meshes, and tubes were quantified and averaged to evaluate vascular stability (DeCicco-Skinner *et al*, 2014) (Fig 3E and Appendix Fig S2B). The higher valency scaffolds H6, H8, Tet2, Icos1, and Icos2 enhanced vascular stability considerably compared with Ang1 at 48 ( $P < 0.01$ ). H6, Icos1 and Icos2 are significantly better than Ang1 at 72 h ( $P < 0.01$ ) (Fig 3F); Icos1 stabilizes vascular tubules 3-fold and 4-fold better than vehicle and 2.4-fold and 3-fold better than Ang1 at 48- and 72-h timepoints, respectively (Fig 3F). F-domain scaffolds presenting four or fewer SpyCatcher domains—Icos1-A, H3, Tet1-A, Tet1-A.2, C4, and AkC4—stabilized the tubules at levels less than the higher valency scaffolds but in the range of Ang1 and Ang2.

In addition to cell migration and tube formation assays, we also investigated the effect F-domain scaffolds have on cell viability. HUVECs were serum starved for 16 h (Harfouche & Hussain, 2006), with or without H3 or H8 (18 nM of F-domains), and analyzed for viability by measuring the cellular ATP levels (Titer-Glo assay). H8- or 20% FBS-treated cells survive significantly better than H3- or PBS-treated samples (Appendix Fig S2C).

### The signaling profiles of the F-domain scaffolds fall into two broad classes

The phenotypes produced by the different F-domain scaffolds in the assays described thus far are summarized in Fig 3G along with

those of Ang1 and Ang2. The scaffolds fall into two broad groups. The first group, like Ang1, induces AKT phosphorylation and tube formation (top of Fig 3G), while the second group, like Ang2, induces FAK and ERK phosphorylation but not Akt phosphorylation and tube formation (bottom part of Fig 3G). The first group contains

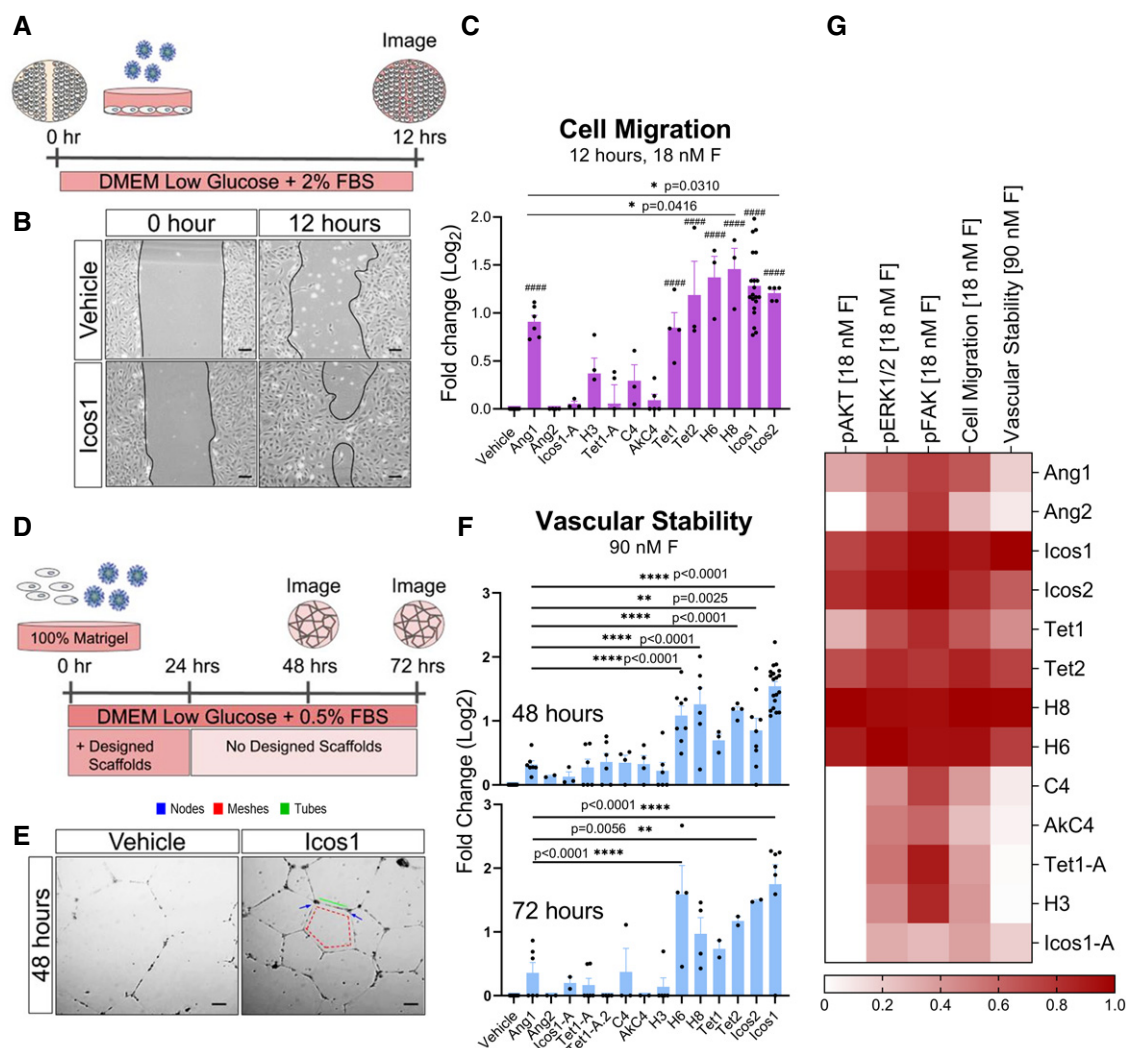


**Figure 3. Designed scaffolds fall into Ang1- or Ang2-like classes depending on valency.**

- A Schematic representation of the *in vitro* scratch cell migration/ wound-healing assay.
- B Icos1 at 18 nM F-domain stimulates cell migration relative to PBS/vehicle control. Scale bars are 100  $\mu$ m.
- C Comparison of cell migration induced by Ang1, Ang2, and designed F-domain scaffolds after 12 h of treatment. The change in wound area was normalized to vehicle control. All experiments have at least three biological replicates. (\*) is the comparison between F-domain scaffolds vs. Ang1, and (#) is the comparison between F-domain scaffolds vs. Vehicle. (####) indicated  $P < 0.0001$ .
- D Schematic of *in vitro* tube formation assay; designed F-domain scaffolds were added at 90 nM F-domain and removed after 24 h; vascular stability was analyzed at 48-h and 72-h timepoints.
- E Representative increase in vascular stability by Icos1. The number of nodes (blue), meshes (red), and tubes (green) was quantified using angiogenesis analyzer plug-in in ImageJ. Scale bar is 100  $\mu$ m.
- F Effect of F-domain scaffolds on the vascular stability at 48- and 72-h timepoints was assessed by taking the average of the number of nodes, meshes, and tubes and normalized to vehicle as log<sub>2</sub> fold change. All experiments have at least three biological replicates except for Ang2 at 48-h timepoint and Ang2, Tet1, Tet2, akC4, and Icos2 at 72-h timepoint in tube formation assay that have two biological replicates.
- G Designed F-domain scaffolds fall into Ang1- and Ang2-like classes. Color indicates highest (1) to lowest (0) pAKT, pERK1/2, and pFAK levels which were column normalized. Cell migration level and vascular stability (48-h timepoint) were also column normalized from highest to lowest.

Data information: In C and F, the bars represent the mean  $\pm$  SEM. One-way ANOVA with Bonferroni test was used for multiple comparisons to calculate  $P$ -values.  $P$ -values are also indicated in Appendix Table S2.

all of the scaffolds presenting six or more SpyCatcher domains, and the second group contains all of the scaffolds with four or fewer domains. This suggests that there are two primary modes of signaling through the Tie2 receptor and that the signaling output produced by a Tie2 agonist depends primarily on its F-domain valency: High valency F-domains lead to an Ang1-like phenotype, while 3–4 F-domains produce an Ang2-like phenotype (Appendix Fig S3). While valency is the dominant determinant of signaling output, the geometry of Tie2 clustering does also appear to play a role; for example, the lower valency scaffolds differ somewhat in the induction of FAK phosphorylation, ERK phosphorylation, and vascular stability.

### High valency F-domain scaffolds result in Tie2/ $\alpha$ 5 $\beta$ 1 integrin superclusters

Ang1, but not Ang2, activates pAKT which phosphorylates FOXO1 and induces translocation out of the nucleus in endothelial cells, modulating endothelial cell gene expression (Brunet *et al*, 1999; Kim *et al*, 2000b, 2016; Daly *et al*, 2004; Han *et al*, 2016). We found that H8, but not H3, also induces FOXO1 nuclear exclusion (Fig 4A–D and Appendix Fig S5C and D).

Ang1 has been suggested to induce Tie2 receptor superclustering (Davis *et al*, 2003; Cho *et al*, 2004; Saharinen *et al*, 2008; Han *et al*, 2016), and hence, we studied the effect of the F-domain scaffolds on Tie2 localization in the plasma membrane by immunofluorescence coupled to confocal and super-resolution microscopy. We found that the H8 scaffold, but not the H3 scaffold, induces dramatic clustering of Tie2 receptors on the cell surface (Fig 4E; Appendix Fig S5E–I). We analyzed these Tie2 clusters using super-resolution microscopy (OMX) and found that Tie2 clusters were associated with dramatic cytoskeletal rearrangements. Cells treated with H8 show actin protrusions with Tie2 clusters at the leading tip of the extensions; such morphology is absent in H3-treated cells (Fig 4F–H). One hypothesis to explain these actin protrusions is that H8 induces HUVEC cell cytoskeletal rearrangements that mimic the cytoskeletal changes observed previously in endothelial cell sprouting (Kobizek *et al*, 1998; Kim *et al*, 2000a; Lee *et al*, 2013).

A plausible mechanistic origin for the differences between the higher valency scaffolds that produce Ang1-like phenotypes and the lower valency scaffolds that produce Ang2-like phenotypes could be the difference in their ability to induce Tie2 superclusters. Receptor clustering, perhaps resulting in liquid–liquid phase transition (Su *et al*, 2016; Boeynaems *et al*, 2018; Case *et al*, 2019), will be favored by higher valency ligands which bring together larger numbers of receptors; for scaffolds with valencies at the borderline between clustering and not clustering, the geometry of receptor engagement may be more of a determining feature and account for the differences in pathway activation observed with lower valency scaffolds.

We took advantage of the observation that H8 induces Tie2 receptor superclustering and investigated the distribution of  $\alpha$ 5 $\beta$ 1 integrins, previously found to interact with and/or modulate Tie2 signaling (Cascone *et al*, 2005; Avraamides *et al*, 2008; Dalton *et al*, 2016; Pang *et al*, 2018). We found that the  $\alpha$ 5 $\beta$ 1 integrin localizes with Tie2 in the Tie2 superclusters induced by the H8 scaffold (Appendix Fig S5J–M). To pursue this observation further, we took advantage of previously developed two-component self-assembling

sheet designs that contained F-domains and GFP (Ben-Sasson *et al*, 2021). Sheet-induced Tie2 clusters were invariably associated with dramatic accumulation of integrin (Fig 4I and J). To explore the signaling importance of the Tie2-integrin interaction, we knocked down  $\alpha$ 5 using siRNA. We observed that pAKT levels were reduced in H8-treated cells in the  $\alpha$ 5 knockdown compared with H8-treated wild-type cells, suggesting that integrin is required for proper Tie2 activity (Fig 4K and L). Tie2 interactions with  $\alpha$ 5 $\beta$ 1 have been found to accelerate cell migration (Pang *et al*, 2018), and these interactions may play a role in the enhancement of migration we observe with the high valency F-domain scaffolds (Fig 3C).

### Icosahedral F-domain scaffolds increase Tie2/Akt signaling after injury and mitigates blood–brain barrier dysfunction

It is notable (Fig 3G and Appendix Fig S1E) that many of the multi-valent scaffolds showed greater Tie2 activation than Ang1. We chose Icos1, one of the high valency scaffolds that gave stabilization of tubules at 48 and 72 h (Fig 3F), to determine whether the super-agonist behavior carries over to the *in vivo* situation to affect vascular function after traumatic injury. Recent studies have highlighted the progressive microvascular damage that spreads from the primary traumatic brain injury (TBI) and openings in the blood–brain barrier (BBB) to become sites of chronic inflammation and areas of progressive white matter damage (Lin *et al*, 1998; Zlokovic, 2011; Glushakova *et al*, 2014). Moreover, attenuation of the Ang/Tie2 pathway has been shown to play a critical role in the loss of neuronal survival and function after TBI in aged animals (Ge *et al*, 2014; Han *et al*, 2014; Brickler *et al*, 2018). We investigated the effect of Icos1 super-agonist administration after a controlled cortical impact injury (CCI-TBI) in adult mice (6 months old). After a mild CCI-TBI, Icos1 or control nanoparticles lacking F-domains (Icos1 $\emptyset$ ) were administered by bolus *i.v.* injection (1.0 mg/kg) at 6, 24, 48, and 72 h post-injury (Fig 5A). On day 4, animals were injected (*i.v.*) with Evans blue to quantify extravasation into the brain parenchyma as a metric for BBB dysfunction and microvascular breakdown (Liu *et al*, 2010; Brickler *et al*, 2018). A marked difference in treatment groups could be seen upon dissection of brain tissue and in serial tissue sections. Animals treated with Tie2 super-agonist Icos1 showed reduced Evans blue tissue penetrance and lesion expansion (Fig 5A and B); Icos1-treated animals showed a significant, 1.7-fold reduction of Evans blue fluorescence in brain extracts derived from both ipsi- and contralateral hemispheres compared with Icos1 $\emptyset$  controls (Fig 5C; 805 vs. 1,375 MFI/g,  $P < 0.0001$ ; 719 vs. 1,036 MFI/g, respectively,  $P = 0.015$ ,  $n = 6$ ).

Secondary neurodegeneration and lesion expansion after CCI-TBI has been attributed to significant loss of microvasculature, chronic microbleeds, and BBB dysfunction that spreads from the primary injury (Allen & Bayraktutan, 2009; Glushakova *et al*, 2014; Wang *et al*, 2016; Salehi *et al*, 2017). Histological analysis of a second cohort of CCI-TBI animals was performed on tissues stained to visualize reactive astrocytes (GFAP stain), microglia (Iba1 stain), and albumin to visualize tissue margins, and brain tissue loss was quantified as a function of lesion surface area between albumin highlighted tissue margins within serial sections of the CCI lesion (Fig 5D, highlighted with white-dotted outline). As before, male and female animals were normalized against body mass to account for animal size-based differences. We observed a 3.5-fold increase in

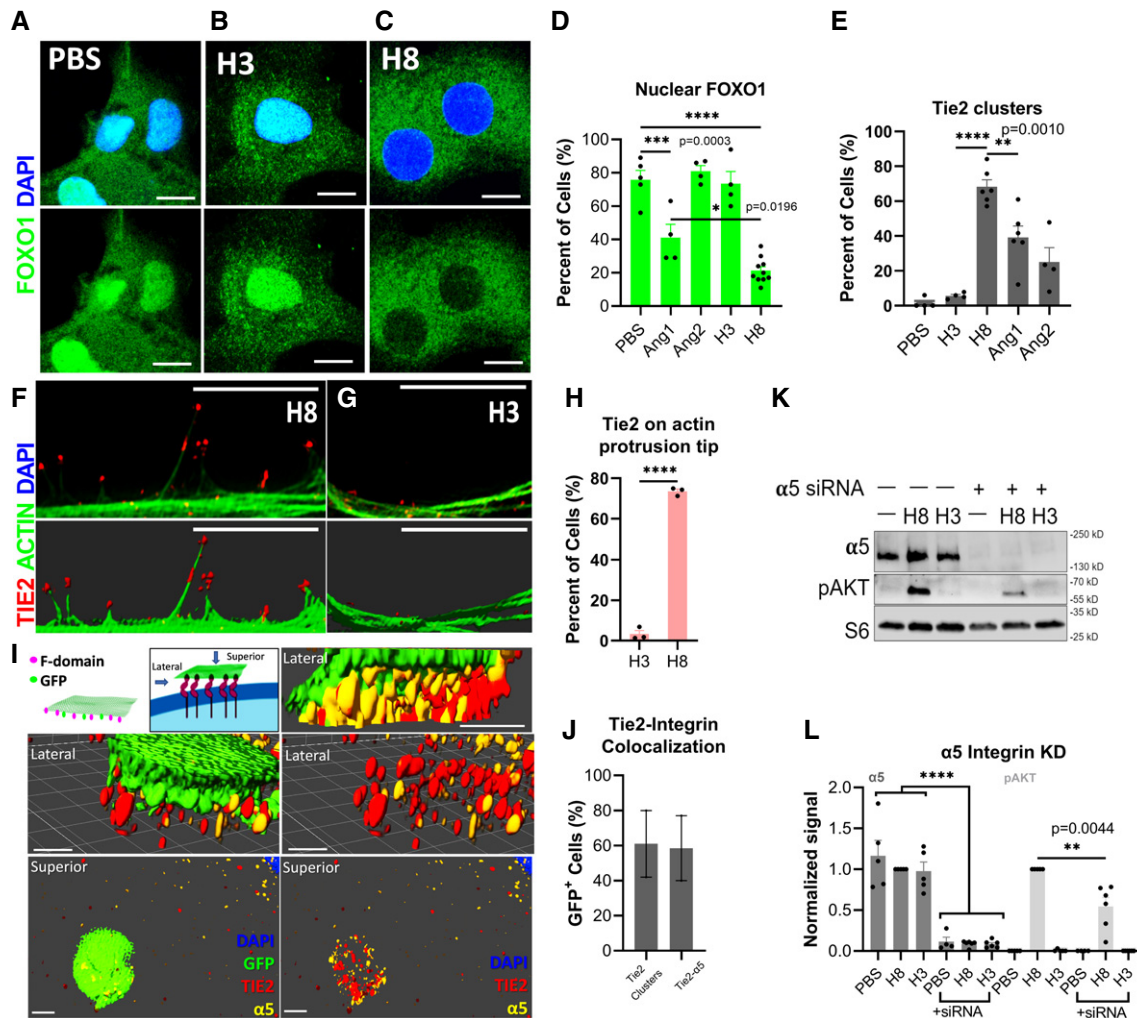


**Figure 4. Tie2 super-agonist generates large Tie2 clusters and initiates cytoskeleton rearrangement.**

Serum-starved HUVECs were treated with angiopoietins or F-domain scaffolds at 100 nM of F-domain concentrations for 15 min before cell fixation and immunofluorescence stained to visualize FOXO1, Tie2, and  $\alpha 5$  integrin.

A–C Representative images of FOXO1 localization upon scaffold administration. Scale bars are 10  $\mu$ m.

D Quantification of nuclear FOXO1 shown as percent of cells with nuclear FOXO1 stain, 100 cells were counted per sample.

E Cells were stimulated with scaffolds or angiopoietins and stained with Tie2 antibodies for analyzing plasma membrane Tie2 clusters. Quantification shows the percent % of total cells that exhibit large Tie2 clusters on the plasma membrane.

F, G H8- or H3-treated cells were analyzed under super-resolution microscopy shows actin protrusions with Tie2 clusters at the tip. Lower panels are Imaris reconstructed 3D model of the super-resolution images. Scale bars are 5  $\mu$ m.

H Quantification of percent of cells exhibited actin protrusions with Tie2 clusters at the tip. 100 cells were counted per sample.

I Tie2-integrin colocalizing upon F-domain sheet stimulation at 18 nM of F-domains for 30 min before fixation and immunofluorescence stained for Tie2 and  $\alpha 5$ . Top right: schematic of F-domain sheet labeled with GFP. Imaris reconstructed super-resolution images of F-domain sheet attaching to cell, clustering Tie2, and inducing  $\alpha 5$  integrin colocalization. Scale bars are 1  $\mu$ m.

J Quantification of Tie2-integrin colocalization for cells that have F-domain sheet (GFP<sup>+</sup>) attachment.

K, L Representatives immunoblot gel (K) and quantifications (L) for  $\alpha 5$  integrin knockdown experiments using 40 nM of siRNA.

Data information: Each point on all graphs represents a biological replicate,  $n > 3$ , and bars represent the mean  $\pm$  SEM. One-way ANOVA with Bonferroni test was used for multiple comparisons to calculate  $P$ -values, and  $t$ -test was used for H. (\*\*\*\*) indicates  $P < 0.0001$ .

lesion expansion (i.e., tissue loss) in Icos1 $\theta$  versus Icos1 nanoparticle treatment (0.771 mm<sup>2</sup> vs. 0.288 mm<sup>2</sup>, respectively;  $P = 0.04$ ,  $n = 4$ ) (Fig 5E). To examine the effects of super-agonist treatment further, we quantified the area stained by albumin extravasation into the brain parenchyma to measure the cumulative effects of neurovascular dysfunction after CCI-TBI. We performed an

unbiased threshold intensity mask overlay analysis on serial tissue sections centered at the CCI lesion and quantified cumulative post-injury neurovascular breakdown as a function of the area stained by serum albumin extravasation within the ipsi-lateral hemisphere (Fig 5F, image insets). Control-treated (Icos1 $\theta$ ) animals showed extensive serum albumin extravasation throughout the injured

brain, whereas albumin levels in the parenchyma of Icos1-treated animals were attenuated 50% ( $3.3 \times 10^6 \mu\text{m}^2$  vs.  $1.7 \times 10^6 \mu\text{m}^2$ , respectively;  $P = 0.01$ ,  $n = 4$ , Fig 5F). Thus, Icos1 super-agonist treatment reduced secondary tissue loss and albumin accumulation after CCI-TBI, which is consistent with the observed increase in BBB integrity.

Due to the significant increases in tissue sparing and reduced serum extravasation in Icos1-treated animals, we next investigated whether super-agonist treatment preserved neurovasculature after injury. CCI-TBI tissue sections were stained to visualize vascular endothelium (CD31 stain) among reactive glia (GFAP stain; Fig 5G) and measure the average diameter of CD31<sup>+</sup> vascular profiles (Fig 5H inset images). As shown, Icos1 administration resulted in marked increase in vessel diameter compared with Icos1 $\emptyset$ -treatment ( $10.4 \mu\text{m} \pm 0.4$  from  $8.7 \mu\text{m} \pm 0.3$ ;  $P = 0.003$ ,  $n = 4$ ; Fig 5H). The number of CD31<sup>+</sup> vessels in adjacent tissue sections of Icos1-treated animals displayed a 30% increase in neurovasculature within 100  $\mu\text{m}$  of the lesion interface ( $302.8 \pm 19.47$  per  $\text{mm}^2$ ) vs. Icos1 $\emptyset$ -controls ( $212.8 \pm 11.14$  per  $\text{mm}^2$ ;  $P = 0.007$ ,  $n = 4$ ; Fig 5I), which is a hallmark of vascular repair (Rosenstein *et al*, 1998; Tang *et al*, 2007; Ogle *et al*, 2014; Sok *et al*, 2017). Interestingly, Tie2 gain-of-function mutations have been shown to correlate with dilated venous formations (Vikkula *et al*, 1996).

Pericytes are specialized mural cells that stabilize capillaries as part of the neurovascular unit and comprise a vital part of the BBB by regulating the integration between astrocytes and endothelial cells (Armulik *et al*, 2010). Moreover, NG2<sup>+</sup>-pericytes have been shown to play a vital role in the stabilization and structure of blood vessels after brain injury, which has been correlated with pAKT upregulation in recovering blood vessels (Teichert *et al*, 2017; Koh *et al*, 2020). We examined the morphology of NG2<sup>+</sup>-pericytes and their association with the CD31<sup>+</sup> vasculature as a measure of BBB integrity (Hartmann *et al*, 2015). Confocal micrographs of CCI-TBI animals treated with Icos1 $\emptyset$  revealed that pericyte localization with CD31 endothelial cells was altered in comparison with Icos1-treated animals (Fig 5J). Icos1 $\emptyset$ -treated brains revealed NG2 proteoglycan deposition in the extracellular matrix was elevated, as were ramified NG2<sup>+</sup>-neuroglia and early glial scarring around remnant CD31 vessels at the injury site (Fig 5J, Icos1 $\emptyset$  and insets, red arrows). In contrast, tissue from Icos1-treated animals showed NG2<sup>+</sup>-pericytes (Fig 5J, yellow) and pAKT (Fig 5J, magenta) colocalization (cyan arrows) throughout the CCI-TBI lesion. Furthermore, NG2 pericytes prominently displayed long lacy processes that were distinct and integrated along CD31 vessels (Fig 5J, Icos1, cyan arrows), which has previously been shown to be correlate with pericyte Tie2 activation and the repair of injured capillaries (Berthiaume *et al*, 2018; Hu *et al*, 2019). Notably, in comparison to Icos1 $\emptyset$ , Icos1 nanocages enhanced Tie2 activation throughout the injury along CD31 vessels (Appendix Fig S6A, B, D and E). Moreover, Icos1-treated tissue showed prevalent phospho-Tie2 colocalization on pericytes with processes that extended along vascular elements (Appendix Fig S6C and F: elongated NG2<sup>+</sup>pTie2<sup>+</sup> processes CD31 vessels). Importantly, Tie2 activation with super-agonist treatment was only noted in tissue proximal to the site of injury, whereas pTie2/pAKT immunostaining in contralateral brain tissue was similar in Icos1 and Icos1 $\emptyset$  controls (Appendix Fig S7A–D). Thus, drug delivery to the brain was a function of injury-dependent vascular permeability and not a result of delivery across an intact BBB. Tie2 super-agonists activate

Tie2 signaling and phospho-Akt in NG2<sup>+</sup>-pericytes to form a critical barrier and cluster around vasculature (Fig 5I, Icos1, inset), which could provide a much needed therapeutic to stabilize BBB function and reduce the side effects of neurovascular dysfunction and traumatic injury to the CNS.

## Discussion

Our systematic examination of Tie2 signaling induced by F-domain scaffolds across a wide range of valencies addresses a long-standing question about the role of ligand valency in determining Tie2 receptor signaling output. As noted earlier, because the native ligands Ang1 and Ang2 populate multiple oligomerization states (Kim *et al*, 2000b, 2005; Davis *et al*, 2003), delineating the role of valency has been difficult. The efficiency of coupling of F-domain SpyTag to all but the tetrameric scaffolds was 90% or greater, and while there is hence some uncertainty in the exact number of F-domains on each construct (for example, for the icosahedral assemblies, between 54 and 60 copies), there are clear overall trends. Scaffolds displaying three or fewer F-domains induce FAK and ERK phosphorylation, but not AKT phosphorylation. In contrast, scaffolds displaying six or more F-domains induce AKT phosphorylation along with FAK and ERK phosphorylation. We observe similar levels of activation with cyclic scaffolds with six F-domains and icosahedral scaffolds with close to 60 F-domains, suggesting that clustering more than 6–8 Tie2 receptors does not further increase signaling. Our experiments also illuminate the inhibition of Ang1 activity by Ang2: scaffolds with three or fewer domains reduce Ang1 activation of AKT signaling, suggesting that inhibition results from direct competition for occupancy of Tie2 receptors. The stability and homogeneity of our F-domain scaffolds should facilitate the determination of the biochemical basis for the F-domain valency-dependent signaling bifurcation; an attractive hypothesis is that the recruitment of PI3K (Kim *et al*, 2000b) to the signaling complexes is Tie2 cluster size-dependent.

Our work complements previous studies of the role of oligomerization in Ang/Tie2 signaling, and by systematically varying geometry and valency of F-domain presentation on a large number of robustly designed scaffolds helps to definitively resolve this issue. Davis *et al* (2003) studied the effects of Fc dimers fused to 1 or 2 copies of the Ang1 or Ang2 F-domain on Tie2 receptor autophosphorylation (resulting in dimeric ligands with 2 or 4 F-domains), but not on downstream signaling, and concluded that four copies of the Ang1 F-domain, but not the Ang2 F-domain, are required in endothelial cells. Tie2 is now known to be phosphorylated on multiple sites, and the relative degree of phosphorylation on the AKT, ERK, and FAK branches of the pathway can differ, as shown in detail here. We do observe some geometry dependence in response to the ligands with smaller numbers of copies, which may explain the F-domain dependence observed by Davis *et al* (2003). Cho *et al* used cartilage oligomeric matrix protein coiled-coil fusions to the F-domain (“Comp-Ang”) that populate both tetrameric and pentameric states, and observe activation of downstream signaling; this suggests that five copies may be sufficient (Cho *et al*, 2004), but as larger assemblies were not tested, it is unclear whether such constructs maximize signaling. The same authors later report that “COMP-Ang1 is quite difficult to use for therapeutic purposes such

as treating sepsis through systemic administration in a controlled manner because of its very short half-life and strong non-specific binding to any tissue (Cho *et al*, 2005; Han *et al*, 2016; Kim *et al*, 2019). Thus, a superior alternative Tie2 agonist has long been

sought for systemic use" (Han *et al*, 2016). The cartilage oligomeric matrix protein variant coiled coils are known to adopt multiple oligomerization states; the much more robust and extensive set of computationally designed scaffolds used in our study enable both

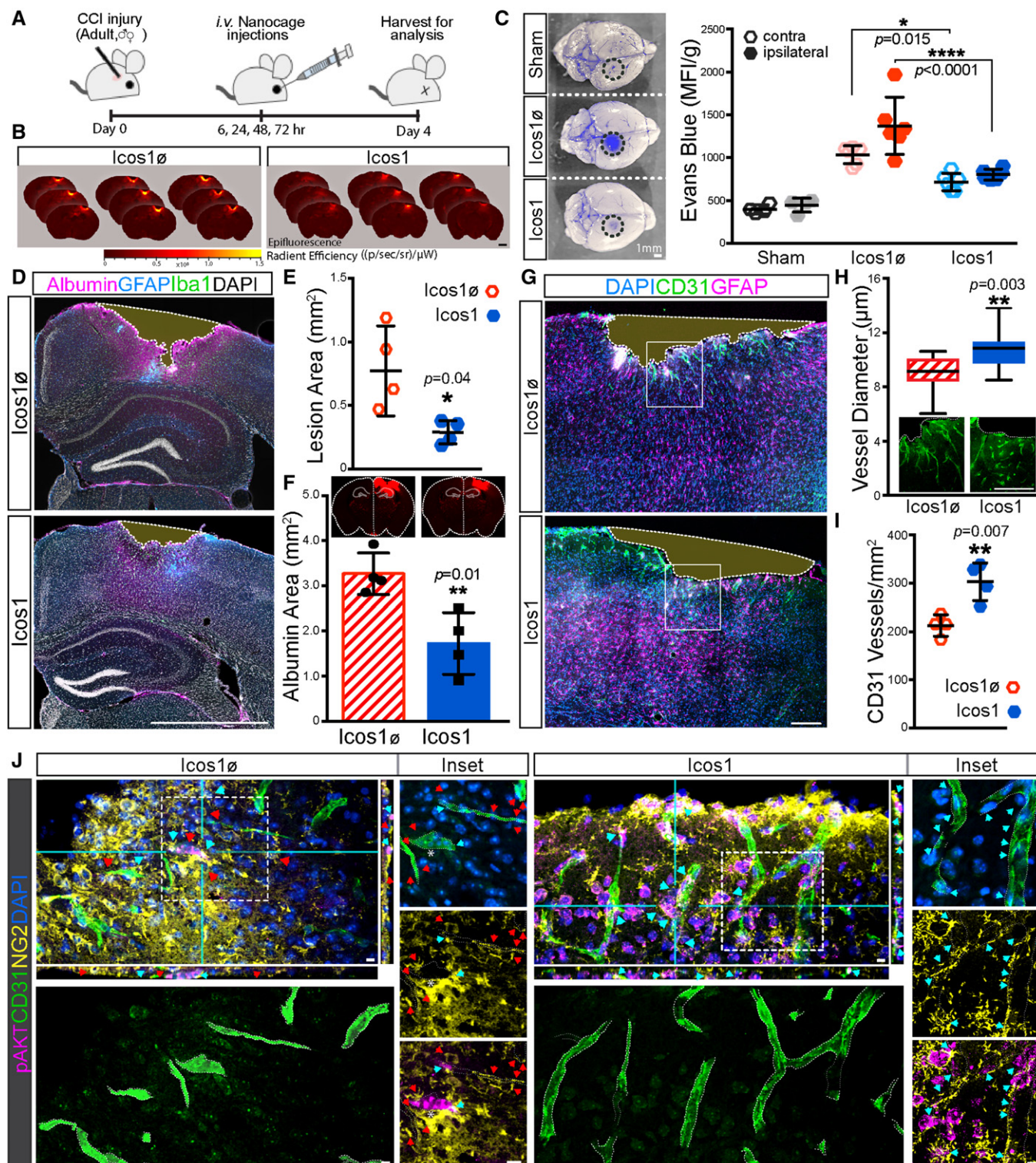


Figure 5.

**Figure 5. Icosahedral F-domain scaffold restores BBB function and enhances angiogenesis after injury.**

- A Brain tissue from CCI-TBI animals injected with Evans blue (5% in saline) after Sham, Icos1 $\emptyset$  (control), or Icos1 (Tie2 super-agonist) injection at 6, 24, 48, and 72 h post-injury was harvested 4 days post-injury.
- B Evans Blue epifluorescence was imaged in serial sections (30  $\mu$ m) through the CCI-TBI lesion to visualize tissue penetrance and lesion spread in Icos1 $\emptyset$ - and Icos1-treated animals. Scale bar is 1 mm.
- C Evans blue extravasation in brain tissue (black dotted circle indicates lesion site) was quantified by fluorescence intensity in tissue extracts from hemispheres contra- and ipsilateral to the injury. Intensity measurement from female and male mice was normalized against body mass to report changes in BBB permeability in Icos1 $\emptyset$ - and Icos1-treated animals ( $P = 0.015$ ,  $P < 0.0001$ ;  $n = 6$ ). Scale bar is 1 mm.
- D, E CCI-TBI brain sections were stained for reactive astrocytes (GFAP, blue), microglia (Iba1, green), and serum albumin (magenta) to highlight tissue margins (dotted white line) and quantify secondary damage as a function of lesion area (E;  $*P = 0.04$ ,  $n = 4$ , the mean  $\pm$  SEM is plotted). Bar, 1 mm.
- F Cumulative blood extravasation into brain tissue (white outline) was imaged by albumin immunofluorescence to establish an unbiased intensity-threshold mask (red) and quantify the area of blood serum extravasation ( $\text{mm}^2$ ) in Icos1 $\emptyset$ - vs. Icos1-treated animals ( $**P = 0.01$ ,  $n = 4$ , the mean  $\pm$  SEM is plotted). Scale bar is 500  $\mu$ m.
- G–I Brain tissues stained by GFAP (magenta) and CD31 immunofluorescence (green) were imaged by confocal microscopy to measure angiogenesis as a function of vessel diameter (H;  $**P = 0.003$ ,  $n = 4$ , the boxes show 25<sup>th</sup> to 75<sup>th</sup> percentiles, and whiskers represent the min and max values.) and quantify the number of CD31 vessels (I;  $**P = 0.007$ ,  $n = 4$ , the mean  $\pm$  SEM is plotted) at the site of injury in Icos1 $\emptyset$ - and Icos1-treated animals 4 days post-injury. Scale bars in G and H is 100  $\mu$ m.
- J Activation of pAKT (Magenta) was examined in Icos1 $\emptyset$ - and Icos1-treated animals within or around vascular (CD31<sup>+</sup>, green) and pericytes (NG2<sup>+</sup> cells, yellow) of the BBB. High-resolution confocal images (insets) reveal the prevalence of activated pAKT (magenta) co-stain (cyan arrows) in pericytes (yellow) of the BBB along vasculature (green, or dotted outline) versus reactive neuroglia (NG2<sup>+</sup>pAKT<sup>-</sup>) in the parenchyma (red arrows) in Icos1 $\emptyset$ - vs. Icos1-treated animals. Scale bar is 10  $\mu$ m.

Data information: One-way ANOVA with Dunnett's test was used for multiple comparisons, and a *t*-test was used to compare two groups.

informed conclusions about the effects of oligomerization state on signaling and likely better pharmacological properties.

Our observation that high valency scaffolds such as H8, but not lower valency scaffolds such as H3, drive Tie2 superclustering suggests that the mechanistic origins of the differences in signaling between the high and low valency scaffolds may be in their ability to associate with a sufficient number of receptors to drive high-order clustering. We also observe  $\alpha 5\beta 1$  integrin in these clusters, and as it has been suggested that Ang1 may interact directly with this integrin, we cannot exclude the possibility that such interactions contribute to the Tie2/ $\alpha 5\beta 1$  superclustering produced by the higher valency F-domain scaffolds (this would require compounds which specifically block F-domain-integrin interactions, which have not been described). We also cannot exclude the possibility that F-domain binding to Tie2 has consequences beyond simple receptor engagement, for example, inducing a conformational change that could modulate interaction with integrins; indeed, it has been reported that engagement of Tie2 by the F-domains of Ang1 and Ang2 can produce different downstream effects (Procopio *et al*, 1999; Kim *et al*, 2009, 2016; Yuan *et al*, 2009; Gerald *et al*, 2013; Han *et al*, 2016). Despite these uncertainties, our results with the series of synthetic ligands unequivocally demonstrate that Ang1 F-domain valency alone is sufficient to determine the outcome of signaling through the Ang/Tie2 pathway.

The latent effects of TBI initiate a cascade of events (Logsdon *et al*, 2015; Iturria-Medina *et al*, 2016; Salehi *et al*, 2017) that contribute to chronic deficits and disease progression that is linked with vascular dysfunction (Kamper *et al*, 2013; Pop *et al*, 2014; Moretti *et al*, 2015). The vascular damage associated with TBI further disrupts the BBB in both the acute (Povlishock *et al*, 1978; Shreiber *et al*, 1999; Habgood *et al*, 2007) and chronic post-injury phase (Cortez *et al*, 1989; Bařkaya *et al*, 1997) because of microbleeds that form sites of persistent neuroinflammation and Wallerian degeneration (Glushakova *et al*, 2014). In a model of acute CCI-TBI, we demonstrate that secondary injury and tissue loss is significantly reduced in animals treated with a Tie2 super-agonist drug. In

accordance with prior studies that have demonstrated angiopoietins promote vascular stabilization after injury (Thurston *et al*, 2000; Zhang *et al*, 2002; Valable *et al*, 2005; Zacharek *et al*, 2007), our Tie2 super-agonist drug formulation increased Tie2/Akt activation and reduced microvascular damage *in vivo*. Our data demonstrate the potential to utilize Tie2 super-agonist drugs as a treatment for enhancing neurovascular function after CCI-TBI; whether these effects avert chronic secondary injury to mitigate disease progression after traumatic injury will require further experimentation.

The capability of designing ligands that can differentially activate branches of Tie2 RTK pathway has implications for treating conditions that require the formation of neovasculature, such as ischemic limb injury, or the stabilization of leaky vasculature and neurovasculature. The potential therapeutic advantages of our defined oligomerization state agonists are highlighted by comparison to Ang1 and Ang2 for which a mixture of oligomerization states are likely to be present (dimers, trimers, and pentamers) which our results suggest will to some extent counteract each other (Cho *et al*, 2004; Oh *et al*, 2015; Han *et al*, 2016). The Ang/Tie2 pathway, in addition to vascular permeability, also regulates the survival and apoptosis of endothelial cells, and regulates normal and tumorigenic angiogenesis and protects stem cells from injury (Puri *et al*, 1995; Stoeltzing *et al*, 2003; Arai *et al*, 2004; Fukuhara *et al*, 2010; Xing *et al*, 2015). Hence, our synthetic agonists and antagonists of this pathway may provide therapeutic options for cancer treatment as well. More generally, our computational design approach to investigate the role of ligand valency and receptor engagement should be broadly applicable to a wide variety of signaling pathways.

## Materials and Methods

### Designed protein scaffolds

Since the Ang1 and Ang2 F-domains are nearly identical, we hypothesized that the differences in Ang1 and Ang2 signaling stem

from differences in the valency and geometry of Tie2 receptor engagement. Because the range of oligomerization states of Ang1 and Ang2 have been difficult to determine, particularly when engaging Tie2 receptors, we set out to determine the molecular basis for the signaling differences by generating a series of synthetic computationally designed ligands displaying F-domains with a wide range of possible valencies (3, 4, 6, 8, 12, 30, and 60 copies) and geometries (cyclic, tetrahedral, and icosahedral). The designed oligomeric proteins were expressed in *E. coli* as fusions to the SpyCatcher protein domain (Zakeri *et al.*, 2012), and the ang1 F-domain (E280-F498) was secreted from 293F cells using a human siderocalin secretion tag, a hexahistidine purification tag and the SpyTag sequence at the N-terminus. Following cleavage of the secretion and purification tags, the F-domain was conjugated *in vitro* to the designed assemblies through spontaneous intramolecular amide bonds form between SpyCatcher–SpyTag via the Lys and Asp residue side chains (Zakeri *et al.*, 2012) (Fig 1A and Appendix Fig S1A). Protein sequences and details on protein production, purification, and conjugation are available in the methods and supporting information (Appendix Fig S4 and Table S1).

We developed three classes of designed symmetric proteins to serve as scaffolds to control the presentation of the F-domain: helical bundles, homo-oligomers, and protein nanoparticles (Fig 1A). The first class, the helical bundles, are parametrically generated *de novo* proteins that exhibit cyclic symmetry and are stabilized by hydrogen-bond networks across multiple chains (Boyken *et al.*, 2016). In this study, we used trimeric, hexameric, and octameric helical bundles (Xu *et al.*, 2020) with an N-terminal fusion to the SpyCatcher protein to allow for conjugation with the F-domain. These designs are annotated as H3, H6, and H8. The second class, homo-oligomers, are designed helical repeat proteins docked into cyclic configurations and contain computationally designed protein–protein interfaces that drive their association in solution. The two proteins in this category, tpr0C3F (Tet1-A) and tpr1C4F (C4) (Fallas *et al.*, 2017), are composed of three or four identical copies of an idealized tetratricopeptide (tpr) repeat protein, respectively, and contain a C-terminal fusion to the SpyCatcher protein to allow for conjugation with the F-domain. The tpr0C3\_r4 (Tet1-A.2) construct is composed of three identical copies of tpr repeat protein with two additional repeating monomers. We also included a tetrameric protein comprised of four copies of idealized ankyrin repeats (AkC4, pdb id 5HS0). The third class, co-assembling protein nanoparticles that exhibit tetrahedral or icosahedral symmetry, are able to display twelve or sixty copies of the F-domain, respectively. T33\_dn2 is a tetrahedral nanocage consisting of two trimeric proteins based on idealized tpr sequences (pdb id and 5HRZ) and contains a fusion to the N-terminus of the A component to the SpyCatcher protein to allow for conjugation with the F-domain, and we refer to this construct as Tet1. T33\_dn10 is a tetrahedral nanocage consisting of two trimeric proteins: one based on an idealized tpr sequence (pdb id 6V8E) and a *de novo* helical repeat protein (pdb id 5K7V). It contains a fusion to the C-terminus of the *de novo* helical repeat protein to the SpyCatcher protein to allow for conjugation with the F-domain, and we refer to this construct as Tet2. I53-50 is an icosahedral protein nanoparticle, which we refer to as Icos1, composed of a pentameric subunit consisting of 12 copies of pentameric Lumazine synthase RibH2 from *Mesorhizobium loti* (PDB ID 2obx) and 20 copies of trimeric 2-keto-3-deoxy-

6-phosphogluconate (KDPG) aldolase from *Thermotoga Maritima* (PDB ID 1wa3). The version of KDPG aldolase used utilizes a fusion with SpyCatcher protein to allow for covalent conjugation with the SpyTagged F-domain. The trimeric component of Icos1 with three copies of F-domains was also tested, annotated as Icos1-A. A version of the pentameric component containing SpyCatcher was also used, allowing for conjugation and display of an additional 60 copies of F-domain, this construct was designated as Icos1-200%. I53-47 is an icosahedral protein nanoparticle composed of 12 copies of pentameric Lumazine synthase (PDB ID 2obx) and 20 copies of the trimeric macrophage migration inhibitory factor from *Trichinella Spiralis* (PDB ID 1hf0) (Bale *et al.*, 2016). It contains a fusion to the SpyCatcher protein to the pentameric component to allow for conjugation with the F-domain, and it is annotated as Icos2.

Synthetic genes encoding each of the SpyCatcher-designed protein fusions were built in a vector with a standard T7 promoter system and (His)6 tag. The proteins were expressed in *E. coli* and purified by immobilized nickel-affinity chromatography (Ni<sup>2+</sup> IMAC) and size-exclusion chromatography (SEC). SpyTag F-domain was secreted from HEK293F cells as a human siderocalin (hSCN) fusion with a (His)6 tag at the N-terminus of the fusion construct (10.1093/nar/gkr706) and purified by immobilized nickel-affinity chromatography (Ni<sup>2+</sup> IMAC). The SpyTag F-domain was obtained by cleavage of the fusion construct using a TEV site engineered at the C-terminus of the hSCN partner which was captured by a secondary Ni<sup>2+</sup> IMAC purification. The cleaved SpyTag F-domain was further purified using SEC. SpyCatcher fusions were incubated overnight with a 1.5 molar excess of SpyTag F-domain in PBS. The mixture was purified by SEC, and SDS–PAGE gels were used to quantify the efficiency of the reaction (Appendix Fig S4).

## Cell culture

Human Umbilical Vein Endothelial Cells (HUVECs) were acquired from Lonza (C2519AS). Cells were grown on 0.1% gelatin-coated (Sigma, G1890-100G) 35-mm cell culture dish in EGM2 media. Briefly, EGM2 consist of 20% fetal bovine serum (BioWest, S1620), 1% penicillin–streptomycin (Gibco, 15140122), 1% GlutaMAX (Gibco, 35050061), 1% ECGS (endothelial cell growth factor), 1 mM sodium pyruvate (Gibco, 11360070), 7.5 mM HEPES (Gibco, 15630130), 0.08 mg/ml heparin (Fisher BioReagents, 9041-08-1), 0.01% amphotericin B (Gibco, 15290018), a mixture of 1x RPMI 1640 (Gibco, 1875093) with and without glucose (Gibco, 11879020) to reach 5.6 mM glucose concentration in the final volume. Media was filtered through a 0.2- $\mu$ m filter. HUVECs were expanded and serially passaged to reach passage 4 before cryopreservation.

ECGS was extracted from 25 mature whole bovine pituitary glands from Pel-Freez biologicals (Lonza, 57133-2). Pituitary glands were homogenized with 187.5 ml of ice-cold 0.15 M NaCl (Fisher Chemical, CAS7647-14-5) and adjusted to pH 4.5 with HCl (Sigma-Aldrich, 320331). The solution was stirred in cold room for 2 h and then centrifuged at 4,000 RPM for 1 h at 4°C. The supernatant (wine colored) was collected and adjusted to pH 7.6 followed by addition of 0.5 g/100 ml streptomycin sulfate (Sigma, S9137) and stirred in cold room overnight. Next day, the supernatant was

centrifuged at 4,000 RPM for 1 h at 4°C. The supernatant was sterile filtered using a 0.45- $\mu$ m filter and stored at  $-20^{\circ}\text{C}$ .

### Phosphorylation analysis of HUVECs stimulated with designed proteins

One straw of passage 4 HUVECs was thawed in a 35-mm dish and cultured in EGM2 medium until almost 80% confluence is reached. Cells were then passaged 1:4 (passage 6) into four 35-mm plates followed by another 1:2 passage (passage 7) at 80–90% confluence into a total of eight plates. Once cells reach 80% confluence, and EGM2 media was aspirated and rinsed with  $1\times$  PBS (Gibco, 10010023) twice. The cells were then starved by adding 2 ml of DMEM low glucose 1 g/l (Gibco, 11885-084) serum-free media per plate for 16 h. At 16-h timepoint, the media was aspirated. Ang1 (R&D system, 923-AN-025), Ang2 (R&D system, 623-AN-025), or scaffolds were suspended in starvation media at 18 nM F-domain concentration and added to the cells for 15- or 30-min incubation at  $37^{\circ}\text{C}$ . After treatment, the media was aspirated, and cells were washed once with  $1\times$  PBS before harvesting total protein for analysis.

During the course of this study, we observed large variability in the action of Ang2. While all Ang2 lots activate P-FAK and P-ERK, the lots (SUL6118081) with BSA carrier and without trehalose have consistently not activated pAKT. However, in lots that have trehalose (SUL6320031) or are carrier-free (SUL6017031), we sometimes see Ang2 activating pAKT. When we add BSA (Gibco, 15260037) (50  $\mu\text{g}$  BSA to 1  $\mu\text{g}$  Ang2 per 1 ml), as suggested by the manufacturer to carrier-free Ang2, the Ang2 capacity to phosphorylate AKT is highly reduced. BSA can prevent protein aggregation or misfolding (Finn *et al*, 2012). Human serum contains albumin at 35–50 mg/ml; thus, it could play a role in maintaining Ang1 and Ang2 physiological oligomerization states. We propose Ang2 can aggregate into higher order ligand clusters in the absence of physiological amounts of carrier proteins (Harfouche & Hussain, 2006).

### Competition assay

HUVECs were cultured and starved as mentioned in protocol above. At 16-h timepoint the media was aspirated and replaced with fresh DMEM low glucose pre-mixed with 9 nM of Ang1 and scaffolds at 27 or 45 nM F-domains (Maisonpierre *et al*, 1997). The cells were stimulated with treatment for 15 min. After 15 min, the media was aspirated, the cells were washed once with  $1\times$  PBS and total protein was harvested for analysis. All experiments were performed with F-domain scaffolds at 90% conjugation.

### Tie2 or $\alpha 5$ integrin Knockdown

Passage 7 HUVECs at 100,000 cells per 35-mm plate cell density were transfected with 40 nM of siRNA (SMARTpool, Dharmacon, Inc.) targeting Tie2 (siRNA: M-003178-03-0005) or  $\alpha 5$  (siRNA: L-008003-00-0005) mRNA using Lipofectamine Transfection Kit (Invitrogen, 13778-075) in EGM2 media. After 24 h of siRNA incubation, media were changed with fresh EGM2 to allow cell recovery for 24 h before 16 h of serum starvation with low glucose DMEM. Starved HUVECs were treated with scaffolds at 18 nM of F-domain concentrations or PBS for 15 min before protein lysate collection for analysis.

### Total protein isolation

After scaffold treatment, the media was aspirated, and the cells were gently rinsed with  $1\times$  phosphate-buffered saline. Cells were lysed with 130  $\mu\text{l}$  of lysis buffer containing 20 mM Tris-HCl (Sigma-Aldrich, 1185-53-1) (pH 7.5), 150 mM NaCl, 15% glycerol (Sigma-Aldrich, G5516), 1% triton (Sigma-Aldrich, 9002-93-1), 3% SDS (Sigma-Aldrich, 151-21-3), 25 mM  $\beta$ -glycerophosphate (Sigma-Aldrich, 50020-100G), 50 mM NaF (Sigma-Aldrich, 7681-49-4), 10 mM sodium pyrophosphate (Sigma-Aldrich, 13472-36-1), 0.5% orthovanadate (Sigma-Aldrich, 13721-39-6), 1% PMSF (Roche Life Sciences, 329-98-6), 25 U benzonase nuclease (EMD, 70664-10KUN), protease inhibitor cocktail (Pierce™ Protease Inhibitor Mini Tablets, Thermo Scientific, A32963), and phosphatase inhibitor cocktail 2 (Sigma-Aldrich, P5726), respectively, in a tube. Cell lysate was collected in a fresh Eppendorf tube. 43.33  $\mu\text{l}$  of  $4\times$  Laemmle Sample buffer (Bio-Rad, 1610747) containing 10% beta-mercaptoethanol (Sigma-Aldrich, M7522-100) was added to the cell lysate and then heated at  $95^{\circ}\text{C}$  for 10 min. For pTie2 Y992 analysis, cells were lysed with 70  $\mu\text{l}$  of lysis buffer and 23  $\mu\text{l}$  of sample buffer was added before boiling. The boiled samples were either used for Western blot analysis or stored at  $-80^{\circ}\text{C}$ .

### Western blotting

The protein samples were thawed and boiled at  $95^{\circ}\text{C}$  for 10 min. 30  $\mu\text{l}$  of protein sample per well was loaded and separated on a 4–10% SDS-PAGE gel for 30 min at 250 Volt. The proteins were then transferred on a nitrocellulose membrane for 12 min using the semi-dry turbo transfer Western blot apparatus (Bio-Rad, USA). Post-transfer, the membrane was blocked in 5% bovine serum albumin for 1 h. After 1 h, the membrane was probed with the respective antibodies: pAkt-S473 (Cell Signaling, 9271S) at 1:2,000 dilution; pERK1/2 p44/42 (Cell signaling, 4370S) at 1:1,000 dilution; pFAK-Y379 (Cell signaling, 8556S) at 1:5,000 dilution; Tie2 (Cell Signaling, 4224S) at 1:1,000 dilution; pTie2 Y992 (R&D sys., AF2720) at 1:500 dilution;  $\alpha 5$  integrin (Millipore, AB1928) at 1:1,000; and  $\beta$ -Actin (Cell Signaling, 3700S), S6 (Cell Signaling, 2217S), and  $\beta$ -Tubulin (Cell Signaling, 2146S) at 1:10,000 dilution. Membranes with primary antibodies were incubated at  $4^{\circ}\text{C}$ , overnight on a rocker. Next day, the membranes were washed with  $1\times$  TBST (3 times, 10 min interval). For pFAK, pERK1/2, ERK, Tie2,  $\alpha 5$  integrin,  $\beta$ -Actin, S6, and  $\beta$ -Tubulin, the respective HRP-conjugated secondary antibody (Bio-Rad, USA) at 1:10,000 dilution was added and incubated at room temperature for 1 h. For pTie2 (Y992), 1:1,000 secondary antibodies were added for 1-h incubation at room temperature. For pAKT(S473), following washes, the membrane was blocked in 5% milk at room temperature for 1 h and then incubated in the respective HRP-conjugated secondary antibody (1:2,000) prepared in 5% milk for 1 h. All the membranes were washed with  $1\times$  TBST (3 times, 10 min of interval) after secondary antibody incubation and developed using Chemiluminescence developer and imaged using Thermo Scientific CL-XPosure Film or Bio-Rad ChemiDoc Imager. Data were quantified using the ImageJ software to analyze band intensity. Quantifications were done by calculating the peak area for each band using ImageJ. The peak area of the target proteins was divided by the peak area of housekeeping proteins. All signaling levels are normalized to Icos-cage levels as an internal positive control.

### Tube formation assay

Tube formation was done according to previously described protocol with modifications (DeCicco-Skinner *et al*, 2014). Briefly, passage 6 HUVECs were seeded onto 24-well plates precoated (30 min prior to seeding) with 150  $\mu$ l of 100% cold Matrigel (Corning, 356231) at  $1.5 \times 10^5$  cells/well density. HUVECs per well were treated with different scaffolds at 90 nM F-domain concentrations or PBS in low glucose DMEM medium supplemented with 0.5% FBS for 24 h in which old media is aspirated and replaced with fresh media without scaffolds. The cells continue to be incubated up to 72 h. Capillary-like structures were observed, and 20 randomly selected microscopic fields were photographed under Nikon Eclipse Ti scope. Thereafter, these tubular formations were quantified by calculating the number of nodes, meshes, and tubes using angiogenesis analyzer in ImageJ software at terminal time point. Data were normalized to PBS vehicle as  $\log_2$  fold change.

### Scratch assay

Scratch assay was done according to previously published protocol with modifications (Liang *et al*, 2007). Briefly, HUVECs were seeded onto 35 mm, 0.1% gelatin-coated plates and cultured in EGM2. Once a monolayer of cells has been established, a scratch is made on the cell layer using a 200- $\mu$ l pipette tip. Media is changed to DMEM low glucose supplemented with 2% fetal bovine serum. Scaffolds were added into the media at 18 nM F-domain concentrations, and PBS is used negative control. The imaging was performed under phase-contrast microscopy 0 and 12 h. The images quantified using ImageJ software to calculate the change in wound area for 12-h time interval. The change in area was then divided by the original wound area to obtain the ratio of wound healing. The ratios were normalized to PBS vehicle as  $\log_2$  fold change.

### Cell viability assay

Cell viability assay was performed according to previously published protocol with the following modifications (Harfouche & Hussain, 2006). HUVECs were seeded onto 96-well plate precoated with 0.1% gelatin at  $2 \times 10^4$  cells/well. The following day, HUVECs were serum starved using low glucose DMEM with PBS or F-domain scaffolds at 18 nM of F-domain for 16 h. No starvation cells were supplemented with 20% FBS as positive control. Cell viability is examined using CellTiter-Glo Luminescent Cell Viability Assay according to product protocol (Promega, G7570). Luminescent signal was measured using Wallac EnVision multiplate reader. Relative luminescence unit (RLU) was calculated by subtracting the average background signal (wells containing the reagent and media only) from sample wells.

### Animals

Prior to beginning all animal studies, the University of Washington Institutional Animal Care and Use Committee (IACUC) evaluated and approved all procedures and power analysis for comparing independent samples (with and alpha 0.05 and 85% confidence) to ensure the ethical use and treatment of animals. For all TBI

experiments, six-month-old C57bl/6 male and female mice were purchased from the Jackson Laboratory.

### Controlled cortical impact (TBI model)

Prior to CCI-TBI, animals are anesthetized and placed in a stereotactic frame. After a midline incision, the scalp is opened to expose the cranium. A small burr hole is drilled ( $\sim 1$  mm diameter)  $\sim 1.0$ – $1.8$  mm caudal to bregma (1.0 mm medial-lateral) to allow placement of an injury probe over the cortex. A fourth-generation Ohio State University impactor is placed on the dura to a touch force of 2–4 kDyn. To impart a controlled cortical impact, a hit is performed as the probe accelerates 4.3 m/s with a displacement of  $-0.8$  mm and 15 ms dwell (White *et al*, 2010). After injury, the probe is retracted, the bone deficit is repaired with bone wax, the scalp is closed, and the animal is allowed to recover with fluid and analgesic administration in a heated environment. Mixed sex cohorts were used to account for neuroprotective effects of estrogen and progesterone after TBI (O'Connor *et al*, 2005; Guo *et al*, 2006; Engler-Chiurazzi *et al*, 2017). Moreover, estrus cycle effects within the female cohort were controlled for with mixed housing and study completion within one estrus cycle (i.e.,  $\leq 7$  days). Synthetic nanocage drugs were administered by retro-orbital i.v. injection on anesthetized animals at 6, 24, 48, and 72 h post-injury (1.0 mg/kg/day). Animal studies were performed in a manner to randomize injury and cohort selection for each treatment to ensure the study was performed in a double-blinded fashion throughout all data collection and tissue analysis.

### Histology and immunofluorescence

Brain tissue was harvested from euthanized animals exsanguinated by transcardiac perfusion with saline and fixed with 4% paraformaldehyde for histological analysis. Tissues were then cryoprotected by equilibration to 30% sucrose (Fisher, S5-500) and embedded in OCT media (Tissue Tek, Inc., 4583) and cryosectioned. All immunofluorescent stains and tissue processing were performed on serial sections (1:6; 30  $\mu$ m). Tris-buffered saline (TBS, Sigma, 901235) equilibrated tissues were permeabilized (0.3% Triton X-100) and blocked (3% bovine serum albumin, BSA). Primary antibodies diluted in blocking solution were incubated at 4°C overnight: Iba1 (1:500, WAKO, NC9288364), CD31 (1:500, R&D system, AF3628), mouse albumin (1:500, ICL, Inc., GAL-90A), GFAP (1:1,000, Millipore, AB5541M1), NG2 (1:100, Millipore, MAB5384), pAKT S473 (1:200, Cell Signaling, 9271S), and DAPI (Thermo Fisher, 62248). Tissues were washed in 0.1% Tween-20 TBS. Fluorescent secondary antibodies diluted (1:500) in Tween-TBS 2% donkey serum (Jackson Immuno, 017-000-121) were incubated with tissues 2–12 h.

For immunofluorescence imaging of HUVECs, passage 7 cells were seeded on glass coverslips coated with 0.1% gelatin and cultured until confluency. Once confluent, cells were starved for 16 h in low glucose DMEM (1 g/l D-glucose). Then, cells were stimulated with angiopoietins or F-domain scaffolds at 100 nM of F-domain concentration for 15 min before fixing with 4% PFA (EMS, 15710) for 13 min. For F-domain sheet (Ben-Sasson *et al*, 2021) experiments, 20 nM of F-domain was added to the cells for 30 min before fixation. The fixed cells were washed three times at 5 min

each before blocking for 1 h with 3% BSA (VWR, 0332-500G) and 0.1% Triton X-100 (Sigma, T9284-500ML) in PBS while on nutation. The cells were incubated with primary antibody diluted at 1:100 in blocking agent over night: Tie2 (Cell Signaling, catalog #4224S), FOXO1 (Cell Signaling, 2880), and  $\alpha 5$  integrin (Millipore, 1928). After the primary antibody, the cells were washed three times at 5 min each with PBS while on nutation. The cells were then incubated with secondary antibodies (1:200 and 1:100 for Tie2) and phalloidin (1:100, Invitrogen, A12380) diluted in blocking agent for 1 h and 20 min at 37°C. Secondary antibodies were then removed, and cells were washed for three times at 10 min each with PBS on nutation. Coverslips were sealed using VECTASHIELD (Vector laboratories, H-2000-2) upside-down on glass slides for analysis in confocal (Leica) or super-resolution (Delta vision OMX SR) microscopy. Selected OMX images were constructed with Imaris 9.7 to create 3D visualizations.

### Evans blue extravasation

To quantify vascular and blood–brain barrier repair, Evans blue (Sigma-Aldrich, 314-13-6) was injected retro-orbitally (2% w/v in saline, sterile filtered). Tissue was harvested after euthanasia and imaged to visualize topical Evans Blue extravasation. Each brain was divided along midline to separate the left and right hemispheres and incubated in 500  $\mu$ l formamide at 55°C. After 24 h, tissue debris was cleared by centrifugation ( $\geq 13,000$  rcf, 15 min). Evans Blue fluorescent was quantified by a TECAN infinite 200Pro plate-reader (excitation: 620 nm, emission: 680 nm). To account for gender differences, Evans blue fluorescence was normalized to express values as a function of body mass ( $n = 6$ ; 50:50 gender representation). Similarly, brain tissue was imaged on a Xenogen imager to qualitatively examine Evans Blue epifluorescence in serial sections.

### Albumin extravasation

Tissue stained with goat antibodies against serum albumin (Immunology Consultant Lab; 1:500) and imaged by a donkey anti-goat antibody conjugated with AlexaFluor-647 (1:500, Jackson Immuno, 715-605-151). Floating sections were counterstained with 4',6-diamidino-2-phenylindole (DAPI) and mounted on slides. After tissue immunofluorescence was scanned by an Olympus VS120 slide-scanner, serum albumin immunofluorescence was quantified with OlyVIA analysis software (Olympus Life Sciences). Briefly, the areas of the ipsi- and contralateral hemispheres were traced in serial section at the TBI lesion epicenter and 180  $\mu$ m rostral and caudal serial sections. Next, albumin immunofluorescence was set to a minimum intensity-threshold, which remained consistent across all animals to ensure the data were unbiased for each mask-area quantification.

### CD31<sup>+</sup> vessel quantification and analysis

Immunofluorescence of CD31<sup>+</sup> vasculature was quantified across serial (1:6) CCI-TBI brain sections (30  $\mu$ m). Vascular endothelium was stained with a goat antibody against CD31 (R&D Systems, Inc., diluted 1:500) and visualized via a donkey anti-goat antibody conjugated with AlexaFluor-488 (Invitrogen, 1:500). Images of CD31<sup>+</sup>

vessels were used to quantify vasculature within the CCI-TBI lesion. A grid was overlaid on images to quantify vessels within 100  $\mu$ m of the lesion surface and then normalized as a function of the surface area ( $\text{mm}^2$ ) to account for variations in lesion size among males and females. ImageJ software (NIH) was used to measure lesion surface and volume as a function of tissue loss by tracing the lesion face and interpolating the cortical surface. Similarly, vessel diameter was measured on 3–5 sections. The cross-sectional distance between the outer margins of CD31<sup>+</sup>-vessels was measured to report microvascular diameter within 300  $\mu$ m of the lesion surface (ImageJ software) on a 1:6 series, and data are reported as the mean for each animal ( $n = 4$ ).

### Statistical analysis

All quantifications show the mean, and error bars are  $\pm$  SEM. Ordinary one-way ANOVA with *post hoc* test, Bonferroni, or Dunnett test was used for multiple comparisons, and a two-tailed, unpaired *t*-test was used for comparing groups of two using GraphPad Prism. *P*-values < 0.05, 0.01, 0.001, 0.0001 are indicated with \*, \*\*, \*\*\* and \*\*\*\*, respectively. *P*-values are stated in Appendix Table S2.

### Data availability

No data were deposited in public databases.

**Expanded View** for this article is available online.

### Acknowledgements

This work is supported by gift from Hahn Family and partly by grants from the National Institutes of Health R01GM097372, R01GM083867, 1P01GM081619, U01HL099997, U01HL099993 for HR-B; Department of Defense PR203328 for HR-B and DB; NIH/NIDCR #T90 DE021984, TR002318 for YTZ; 5R21NS099654 and 1R01NS118247 for DLS.

### Author contributions

YTZ, JAF, GU, DB, and HR-B planned the experiments and wrote the manuscript; JAF, GU, CX, and DB designed the protein constructs; YTZ, SS, LS, ZZ, IXR, JM, and HR-B performed or designed *in vitro* experiments; JAF, GU, LC, and SW prepared the protein constructs; DLS performed *in vivo* animal study.

### Conflict of interest

The authors declare that they have no conflict of interest.

### References

- Allen C, Bayraktutan U (2009) Oxidative stress and its role in the pathogenesis of ischaemic stroke. *Int J Stroke* 4: 461–470
- Arai F, Hirao A, Ohmura M, Sato H, Matsuoka S, Takubo K, Ito K, Koh GY, Suda T (2004) Tie2/angiopoietin-1 signaling regulates hematopoietic stem cell quiescence in the bone marrow niche. *Cell* 118: 149–161
- Armulik A, Genové G, Mäe M, Nisancioglu MH, Wallgard E, Niaudet C, He L, Norlin J, Lindblom P, Strittmatter K et al (2010) Pericytes regulate the blood-brain barrier. *Nature* 468: 557–561
- Avraamides CJ, Garmy-Susini B, Varner JA (2008) Integrins in angiogenesis and lymphangiogenesis. *Nat Rev Cancer* 8: 604–617

- Bale JB, Gonen S, Liu Y, Sheffler W, Ellis D, Thomas C, Cascio D, Yeates TO, Gonen T, King NP et al (2016) Accurate design of megadalton-scale two-component icosahedral protein complexes. *Science* 353: 389–394
- Barton WA, Tzvetkova-Robev D, Miranda EP, Kolev MV, Rajashankar KR, Himanen JP, Nikolov DB (2006) Crystal structures of the Tie2 receptor ectodomain and the angiotensin-2-Tie2 complex. *Nat Struct Mol Biol* 13: 524–532
- Başkaya MK, Rao AM, DoĐan A, Donaldson D, Dempsey RJ (1997) The biphasic opening of the blood-brain barrier in the cortex and hippocampus after traumatic brain injury in rats. *Neurosci Lett* 226: 33–36
- Ben-Sasson AJ, Watson JL, Sheffler W, Johnson MC, Bittleston A, Somasundaram L, Decarreau J, Jiao F, Chen J, Mela I et al (2021) Design of biologically active binary protein 2D materials. *Nature* 589: 468–473
- Berthiaume AA, Grant RI, McDowell KP, Underly RG, Hartmann DA, Levy M, Bhat NR, Shih AY (2018) Dynamic remodeling of pericytes *in vivo* maintains capillary coverage in the adult mouse brain. *Cell Rep* 22: 8–16
- Boeynaems S, Alberti S, Fawzi NL, Mittag T, Polymenidou M, Rousseau F, Schymkowitz J, Shorter J, Wolozin B, Van Den Bosch L et al (2018) Protein phase separation: a new phase in cell biology. *Trends Cell Biol* 28: 420–435
- Boyken SE, Chen Z, Groves B, Langan RA, Oberdorfer G, Ford A, Gilmore JM, Xu C, DiMaio F, Pereira JH et al (2016) De novo design of protein homo-oligomers with modular hydrogen-bond network-mediated specificity. *Science* 352: 680–687
- Brickler TR, Hazy A, Guilhaume Correa F, Dai R, Kowalski EJA, Dickerson R, Chen J, Wang X, Morton PD, Whittington A et al (2018) Angiotensin/Tie2 axis regulates the age-at-injury cerebrovascular response to traumatic brain injury. *J Neurosci* 38: 9618–9634
- Brunet A, Bonni A, Zigmond MJ, Lin MZ, Juo P, Hu LS, Anderson MJ, Arden KC, Blenis J, Greenberg ME (1999) Akt promotes cell survival by phosphorylating and inhibiting a forkhead transcription factor. *Cell* 96: 857–868
- Cascone I, Napione L, Maniero F, Serini G, Bussolino F (2005) Stable interaction between  $\alpha 5\beta 1$  integrin and Tie2 tyrosine kinase receptor regulates endothelial cell response to Ang-1. *J Cell Biol* 170: 993–1004
- Case LB, Ditlev JA, Rosen MK (2019) Regulation of transmembrane signaling by phase separation. *Annu Rev Biophys* 48: 465–494
- Cho C-H, Kammerer RA, Lee HJ, Steinmetz MO, Ryu YS, Lee SH, Yasunaga K, Kim K-T, Kim I, Choi H-H et al (2004) COMP-Ang1: A designed angiotensin-1 variant with nonleaky angiogenic activity. *Proc Natl Acad Sci USA* 101: 5547–5552
- Cho C-H, Kim KE, Byun J, Jang H-S, Kim D-K, Baluk P, Baffert F, Lee GM, Mochizuki N, Kim J et al (2005) Long-term and sustained COMP-Ang1 induces long-lasting vascular enlargement and enhanced blood flow. *Circ Res* 97: 86–94
- Cortez SC, McIntosh TK, Noble LJ (1989) Experimental fluid percussion brain injury: vascular disruption and neuronal and glial alterations. *Brain Res* 482: 271–282
- Dalton AC, Shlamkovitch T, Papo N, Barton WA (2016) Constitutive association of Tie1 and Tie2 with endothelial integrins is functionally modulated by angiotensin-1 and fibronectin. *PLoS One* 11: e0163732
- Daly C, Wong V, Burova E, Wei Y, Zabski S, Griffiths J, Lai KM, Lin HC, Ioffe E, Yancopoulos GD et al (2004) Angiotensin-1 modulates endothelial cell function and gene expression via the transcription factor FKHR (FOXO1). *Genes Dev* 18: 1060–1071
- Davis S, Papadopoulos N, Aldrich TH, Maisonpierre PC, Huang T, Kovac L, Xu A, Leidich R, Radziejewska E, Rafique A et al (2003) Angiotensins have distinct modular domains essential for receptor binding, dimerization and superclustering. *Nat Struct Biol* 10: 38–44
- DeCicco-Skinner KL, Henry GH, Cataisson C, Tabib T, Gwilliam JC, Watson NJ, Bullwinkle EM, Falkenburg L, O'Neill RC, Morin A et al (2014) Endothelial cell tube formation assay for the *in vitro* study of angiogenesis. *J Vis Exp* e51312
- Engler-Chiurazzi EB, Brown CM, Povroznik JM, Simpkins JW (2017) Estrogens as neuroprotectants: Estrogenic actions in the context of cognitive aging and brain injury. *Prog Neurobiol* 157: 188–211
- Fallas JA, Ueda G, Sheffler W, Nguyen V, McNamara DE, Sankaran B, Pereira JH, Parmeggiani F, Brunette TJ, Cascio D et al (2017) Computational design of self-assembling cyclic protein homo-oligomers. *Nat Chem* 9: 353–360
- Finn TE, Nunez AC, Sunde M, Easterbrook-Smith SB (2012) Serum albumin prevents protein aggregation and amyloid formation and retains chaperone-like activity in the presence of physiological ligands. *J Biol Chem* 287: 21530–21540
- Fukuhara S, Sako K, Minami T, Noda K, Kim HZ, Kodama T, Shibuya M, Takakura N, Koh GY, Mochizuki N (2008) Differential function of Tie2 at cell-cell contacts and cell-substratum contacts regulated by angiotensin-1. *Nat Cell Biol* 10: 513–526
- Fukuhara S, Sako K, Noda K, Zhang J, Minami M, Mochizuki N (2010) Angiotensin-1/Tie2 receptor signaling in vascular quiescence and angiogenesis. *Histol Histopathol* 25: 387–396
- Ge X-T, Lei P, Wang H-C, Zhang A-L, Han Z-L, Chen X, Li S-H, Jiang R-C, Kang C-S, Zhang J-N (2014) miR-21 improves the neurological outcome after traumatic brain injury in rats. *Sci Rep* 4: 6718
- Gerald D, Chintharlapalli S, Augustin HG, Benjamin LE (2013) Angiotensin-2: an attractive target for improved antiangiogenic tumor therapy. *Cancer Res* 73: 1649–1657
- Glushakova OY, Johnson D, Hayes RL (2014) Delayed increases in microvascular pathology after experimental traumatic brain injury are associated with prolonged inflammation, blood-brain barrier disruption, and progressive white matter damage. *J Neurotrauma* 31: 1180–1193
- Guo Q, Sayeed I, Baronne LM, Hoffman SW, Guennoun R, Stein DG (2006) Progesterone administration modulates AQP4 expression and edema after traumatic brain injury in male rats. *Exp Neurol* 198: 469–478
- Habgood MD, Bye N, Dziegielewska KM, Ek CJ, Lane MA, Potter A, Morganti-Kossmann C, Saunders NR (2007) Changes in blood-brain barrier permeability to large and small molecules following traumatic brain injury in mice. *Eur J Neurosci* 25: 231–238
- Han S, Lee S-J, Kim KE, Lee HS, Oh N, Park I, Ko E, Oh SJ, Lee Y-S, Kim D et al (2016) Amelioration of sepsis by TIE2 activation-induced vascular protection. *Sci Transl Med* 8: 335ra55
- Han Z, Chen F, Ge X, Tan J, Lei P, Zhang J (2014) miR-21 alleviated apoptosis of cortical neurons through promoting PTEN-Akt signaling pathway *in vitro* after experimental traumatic brain injury. *Brain Res* 1582: 12–20
- Harfouche R, Hussain SNA (2006) Signaling and regulation of endothelial cell survival by angiotensin-2. *Am J Physiol Heart Circ Physiol* 291: H1635–H1645
- Hartmann DA, Underly RG, Grant RI, Watson AN, Lindner V, Shih AY (2015) Pericyte structure and distribution in the cerebral cortex revealed by high-resolution imaging of transgenic mice. *Neurophotonics* 2: 041402
- Hu E, Hu W, Yang A, Zhou H, Zhou J, Luo J, Wang Y, Tang T, Cui H (2019) Thrombin promotes pericyte coverage by Tie2 activation in a rat model of intracerebral hemorrhage. *Brain Res* 1708: 58–68
- Iturria-Medina Y, Sotero RC, Toussaint PJ, Mateos-Pérez JM, Evans AC, Alzheimer's Disease Neuroimaging Initiative (2016) Early role of vascular

- dysregulation on late-onset Alzheimer's disease based on multifactorial data-driven analysis. *Nat Commun* 7: 11934
- Kamper JE, Pop V, Fukuda AM, Ajao DO, Hartman RE, Badaut J (2013) Juvenile traumatic brain injury evolves into a chronic brain disorder: behavioral and histological changes over 6 months. *Exp Neurol* 250: 8–19
- Kim HZ, Jung K, Kim HM, Cheng Y, Koh GY (2009) A designed angiopoietin-2 variant, pentameric COMP-Ang2, strongly activates Tie2 receptor and stimulates angiogenesis. *Biochim Biophys Acta - Mol Cell Res* 1793: 772–780
- Kim I, Kim HG, Moon S-O, Chae SW, So J-N, Koh KN, Ahn BC, Koh GY (2000a) Angiopoietin-1 induces endothelial cell sprouting through the activation of focal adhesion kinase and plasmin secretion. *Circ Res* 86: 952–959
- Kim I, Kim HG, So JN, Kim JH, Kwak HJ, Koh GY (2000b) Angiopoietin-1 regulates endothelial cell survival through the phosphatidylinositol 3'-kinase/Akt signal transduction pathway. *Circ Res* 86: 24–29
- Kim J, Park JR, Choi J, Park I, Hwang Y, Bae H, Kim Y, Choi W, Yang JM, Han S et al (2019) Tie2 activation promotes choriocapillary regeneration for alleviating neovascular age-related macular degeneration. *Sci Adv* 5: eaau6732
- Kim KT, Choi HH, Steinmetz MO, Maco B, Kammerer RA, Ahn SY, Kim HZ, Lee GM, Koh GY (2005) Oligomerization and multimerization are critical for angiopoietin-1 to bind and phosphorylate Tie2. *J Biol Chem* 280: 20126–20131
- Kim M, Allen B, Korhonen EA, Nitschké M, Yang HW, Baluk P, Saharinen P, Alitalo K, Daly C, Thurston G et al (2016) Opposing actions of angiopoietin-2 on Tie2 signaling and FOXO1 activation. *J Clin Invest* 126: 3511–3525
- Koblizek TI, Weiss C, Yancopoulos GD, Deutsch U, Risau W (1998) Angiopoietin-1 induces sprouting angiogenesis *in vitro*. *Curr Biol* 8: 529–532
- Koh BI, Lee HJ, Kwak PA, Yang MJ, Kim J-H, Kim H-S, Koh GY, Kim I (2020) VEGFR2 signaling drives meningeal vascular regeneration upon head injury. *Nat Commun* 11: 1–17
- Lee J, Kim KE, Choi DK, Jang JY, Jung JJ, Kiyonari H, Shioi G, Chang W, Suda T, Mochizuki N et al (2013) Angiopoietin-1 guides directional angiogenesis through integrin  $\alpha\beta 5$  signaling for recovery of ischemic retinopathy. *Sci Transl Med* 5: 203ra127
- Leppänen VM, Saharinen P, Alitalo K (2017) Structural basis of Tie2 activation and Tie2/Tie1 heterodimerization. *Proc Natl Acad Sci USA* 114: 4376–4381
- Liang CC, Park AY, Guan JL (2007) *In vitro* scratch assay: a convenient and inexpensive method for analysis of cell migration *in vitro*. *Nat Protoc* 2: 329–333
- Lin P, Buxton JA, Acheson A, Radziejewski C, Maisonpierre PC, Yancopoulos GD, Channon KM, Hale LP, Dewhirst MW, George SE et al (1998) Antiangiogenic gene therapy targeting the endothelium-specific receptor tyrosine kinase Tie2. *Proc Natl Acad Sci USA* 95: 8829–8834
- Liu DZ, Ander BP, Xu H, Shen Y, Kaur P, Deng W, Sharp FR (2010) Blood-brain barrier breakdown and repair by Src after thrombin-induced injury. *Ann Neurol* 67: 526–533
- Logsdon AF, Lucke-Wold BP, Turner RC, Huber JD, Rosen CL, Simpkins JW (2015) Role of microvascular disruption in brain damage from traumatic brain injury. *Compr Physiol* 5: 1147–1160
- Maisonpierre PC, Suri C, Jones PF, Bartunkova S, Wiegand SJ, Radziejewski C, Compton D, McClain J, Aldrich TH, Papadopoulos N et al (1997) Angiopoietin-2, a natural antagonist for Tie2 that disrupts *in vivo* angiogenesis. *Science* 277: 55–60
- Mazurek R, Dave JM, Chandran RR, Misra A, Sheikh AQ, Greif DM (2017) Vascular cells in blood vessel wall development and disease. In *Advances in Pharmacology*, Khalil, Raouf A (eds), Vol. 78, pp 323–350. San Diego, CA: Academic Press Inc
- Moore JO, Lemmon MA, Ferguson KM (2017) Dimerization of Tie2 mediated by its membrane-proximal FNIII domains. *Proc Natl Acad Sci USA* 114: 4382–4387
- Moretti R, Pansiot J, Bettati D, Strazielle N, Chersi-Egea JF, Damante G, Fleiss B, Titomanlio L, Gressens P (2015) Blood-brain barrier dysfunction in disorders of the developing brain. *Front Neurosci* 9: 1–15
- O'Connor CA, Cernak I, Vink R (2005) Both estrogen and progesterone attenuate edema formation following diffuse traumatic brain injury in rats. *Brain Res* 1062: 171–174
- Ogle ME, Sefcik LS, Awojoodu AO, Chiappa NF, Lynch K, Peirce-Cottler S, Botchwey EA (2014) Engineering *in vivo* gradients of sphingosine-1-phosphate receptor ligands for localized microvascular remodeling and inflammatory cell positioning. *Acta Biomater* 10: 4704–4714
- Oh N, Kim K, Jin Kim S, Park I, Lee JE, Suk Seo Y, Joo An H, Min Kim H, Young Koh G (2015) A designed angiopoietin-1 variant, dimeric CMP-Ang1 activates Tie2 and stimulates angiogenesis and vascular stabilization in N-glycan dependent manner. *Sci Rep* 5: 15291
- Pang D, Wang L, Dong J, Lai X, Huang Q, Milner R, Li L (2018) Integrin  $\alpha\beta 1$ -Ang1/Tie2 receptor cross-talk regulates brain endothelial cell responses following cerebral ischemia. *Exp Mol Med* 50: 1–12
- Pop R, Manisor M, Wolff V, Habashy M, Rouyer O, Kehrli P, Marescaux C, Beaujeux R (2014) Endovascular treatment in two cases of bilateral ischemic stroke. *Cardiovasc Intervent Radiol* 37: 829–834
- Povlishock JT, Becker DP, Sullivan HG, Miller JD (1978) Vascular permeability alterations to horseradish peroxidase in experimental brain injury. *Brain Res* 153: 223–239
- Procopio WN, Pelavin PI, Lee WMF, Yeilding NM (1999) Angiopoietin-1 and -2 coiled coil domains mediate distinct homo- oligomerization patterns, but fibrinogen-like domains mediate ligand activity. *J Biol Chem* 274: 30196–30201
- Puri MC, Rossant J, Alitalo K, Bernstein A, Partanen J (1995) The receptor tyrosine kinase TIE is required for integrity and survival of vascular endothelial cells. *EMBO J* 14: 5884–5891
- Rosenstein JM, Mani N, Silverman WF, Krum JM (1998) Patterns of brain angiogenesis after vascular endothelial growth factor administration *in vitro* and *in vivo*. *Proc Natl Acad Sci USA* 95: 7086
- Saharinen P, Eklund L, Miettinen J, Wirkkala R, Anisimov A, Winderlich M, Nottebaum A, Vestweber D, Deutsch U, Koh GY et al (2008) Angiopoietins assemble distinct Tie2 signalling complexes in endothelial cell-cell and cell-matrix contacts. *Nat Cell Biol* 10: 527–537
- Salehi A, Zhang JH, Obenaus A (2017) Response of the cerebral vasculature following traumatic brain injury. *J Cereb Blood Flow Metab* 37: 2320–2339
- Shreiber DI, Smith DH, Meaney DF (1999) Immediate *in vivo* response of the cortex and the blood-brain barrier following dynamic cortical deformation in the rat. *Neurosci Lett* 259: 5–8
- Sok MCP, Tria MC, Olingy CE, San Emeterio CL, Botchwey EA (2017) Aspirin-Triggered Resolvin D1-modified materials promote the accumulation of pro-regenerative immune cell subsets and enhance vascular remodeling. *Acta Biomater* 53: 109–122
- Souma T, Tompson SW, Thomson BR, Siggs OM, Kizhatil K, Yamaguchi S, Feng L, Limviphuvadh V, Whisenhunt KN, Maurer-Stroh S et al (2016) Angiopoietin receptor TEK mutations underlie primary congenital glaucoma with variable expressivity. *J Clin Invest* 126: 2575–2587
- Stoeltzing O, Ahmad SA, Liu W, McCarty MF, Wey JS, Parikh AA, Fan F, Reinmuth N, Kawaguchi M, Bucana CD et al (2003) Angiopoietin-1 inhibits

- vascular permeability, angiogenesis, and growth of hepatic colon cancer tumors. *Cancer Res* 63: 3370–3377
- Su X, Ditlev JA, Hui E, Xing W, Banjade S, Okrut J, King DS, Taunton J, Rosen MK, Vale RD (2016) Phase separation of signaling molecules promotes T cell receptor signal transduction. *Science* 352: 595–599
- Tang T, Liu XJ, Zhang ZQ, Zhou HJ, Luo JK, Huang JF, Yang QD, Li XQ (2007) Cerebral angiogenesis after collagenase-induced intracerebral hemorrhage in rats. *Brain Res* 1175: 134–142
- Teichert M, Milde L, Holm A, Stanicek L, Gengenbacher N, Savant S, Ruckdeschel T, Hasanov Z, Srivastava K, Hu J et al (2017) Pericyte-expressed Tie2 controls angiogenesis and vessel maturation. *Nat Commun* 8: 16106
- Thurston G, Rudge JS, Ioffe E, Zhou H, Ross L, Croll SD, Glazer N, Holash J, McDonald DM, Yancopoulos GD (2000) Angiopoietin-1 protects the adult vasculature against plasma leakage. *Nat Med* 6: 460–463
- Valable S, Montaner J, Bellail A, Berezowski V, Brillault J, Cecchelli R, Divoux D, MacKenzie ET, Bernaudin M, Roussel S et al (2005) VEGF-induced BBB permeability is associated with an MMP-9 activity increase in cerebral ischemia: both effects decreased by Ang-1. *J Cereb Blood Flow Metab* 25: 1491–1504
- Vikkula M, Boon LM, Iii KL, Calvert JT, Diamonti AJohn, Goumnerov B, Pasyk KA, Marchuk DA, Warman ML, Cantley LC et al (1996) Vascular dysmorphogenesis caused by an activating mutation in the receptor tyrosine kinase TIE2. *Cell* 87: 1181–1190
- Wang Y, Fan X, Tang T, Fan R, Zhang C, Huang Z, Peng W, Gan P, Xiong X, Huang W et al (2016) Rhein and rhubarb similarly protect the blood-brain barrier after experimental traumatic brain injury via gp91 phox subunit of NADPH oxidase/ROS/ERK/MMP-9 signaling pathway. *Sci Rep* 6
- White BD, Nathe RJ, Maris DO, Nguyen NK, Goodson JM, Moon RT, Horner PJ (2010)  $\beta$ -catenin signaling increases in proliferating NG2 progenitors and astrocytes during post-traumatic gliogenesis in the adult brain. *Stem Cells* 28: 297–307
- Xing Y, Su TT, Ruohola-Baker H (2015) Tie-mediated signal from apoptotic cells protects stem cells in *Drosophila melanogaster*. *Nat Commun* 6: 7058
- Xu C, Lu P, Gamal El-Din TM, Pei XY, Johnson MC, Uyeda A, Bick MJ, Xu QI, Jiang D, Bai H et al (2020) Computational design of transmembrane pores. *Nature* 585: 129–134
- Xue G, Hemmings BA (2013) PKB/akt-dependent regulation of cell motility. *J Natl Cancer Inst* 105: 393–404
- Yu X, Seegar TCM, Dalton AC, Tzvetkova-Robev D, Goldgur Y, Rajashankar KR, Nikolov DB, Barton WA (2013) Structural basis for angiopoietin-1-mediated signaling initiation. *Proc Natl Acad Sci USA* 110: 7205–7210
- Yuan HT, Khankin EV, Karumanchi SA, Parikh SM (2009) Angiopoietin 2 is a partial agonist/antagonist of Tie2 signaling in the endothelium. *Mol Cell Biol* 29: 2011–2022
- Zacharek A, Chen J, Li A, Cui X, Li Y, Roberts C, Feng Y, Gao Q, Chopp M (2007) Angiopoietin1/TIE2 and VEGF/FLK1 induced by MSC treatment amplifies angiogenesis and vascular stabilization after stroke. *J Cereb Blood Flow Metab* 27: 1684–1691
- Zakeri B, Fierer JO, Celik E, Chittock EC, Schwarz-Linek U, Moy VT, Howarth M (2012) Peptide tag forming a rapid covalent bond to a protein, through engineering a bacterial adhesin. *Proc Natl Acad Sci USA* 109: E690–E697
- Zhang ZG, Zhang L, Croll SD, Chopp M (2002) Angiopoietin-1 reduces cerebral blood vessel leakage and ischemic lesion volume after focal cerebral embolic ischemia in mice. *Neuroscience* 113: 683–687
- Zlokovic BV (2011) Neurovascular pathways to neurodegeneration in Alzheimer's disease and other disorders. *Nat Rev Neurosci* 12: 723–738